



# Machine learning for optimal design of circular hollow section stainless steel stub columns: A comparative analysis with Eurocode 3 predictions

Ikram Abarkan<sup>a</sup>, Musab Rabi<sup>b</sup>, Felipe Piana Vendramell Ferreira<sup>c</sup>, Rabee Shamass<sup>d,\*</sup>,  
Vireen Limbachiya<sup>e</sup>, Yazeed S. Jweihan<sup>f</sup>, Luis Fernando Pinho Santos<sup>e</sup>

<sup>a</sup> Department of Physics, Faculty of Sciences, Abdelmalek Essaâdi University, 93002, Tetouan, Morocco

<sup>b</sup> Dept of Civil Engineering, Jerash University, Jordan

<sup>c</sup> Faculty of Civil Engineering, Federal University of Uberlandia – Campus Santa Monica, Uberlandia, Minas Gerais, Brazil

<sup>d</sup> Department of Civil and Environmental Engineering, Brunel University London, London, UK

<sup>e</sup> Division of Civil and Building Services Engineering, School of the Built Environment and Architecture, London South Bank University, UK

<sup>f</sup> Civil and Environmental Engineering Department, College of Engineering, Mutah University, Mutah, Karak, 61710, P.O. BOX 7, Jordan

## ARTICLE INFO

### Keywords:

Circular hollow sections  
Stainless steel  
Finite element model  
Artificial neural network  
Support vector machine regression  
Gene Expression Programming  
Decision Trees for Regression

## ABSTRACT

Stainless steel has many advantages when used in structures, however, the initial cost is high. Hence, it is essential to develop reliable and accurate design methods that can optimize the material. As novel, reliable soft computation methods, machine learning provided more accurate predictions than analytical formulae and solved highly complex problems. The present study aims to develop machine learning models to predict the cross-section resistance of circular hollow section stainless steel stub column. A parametric study is conducted by varying the diameter, thickness, length, and mechanical properties of the column. This database is used to train, validate, and test machine learning models, Artificial Neural Network (ANN), Decision Trees for Regression (DTR), Gene Expression Programming (GEP) and Support Vector Machine Regression (SVMR). Thereafter, results are compared with finite element models and Eurocode 3 (EC3) to assess their accuracy. It was concluded that the EC3 models provided conservative predictions with an average Predicted-to-Actual ratio of 0.698 and Root Mean Square Error (RMSE) of 437.3. The machine learning models presented the highest level of accuracy. However, the SVMR model based on RBF kernel presented a better performance than the ANN, GEP and DTR machine learning models, and RMSE value for SVMR, ANN, GEP and DTR is 22.6, 31.6, 152.84 and 29.07, respectively. The GEP leads to the lowest level of accuracy among the other three machine learning models, yet, it is more accurate than EC3. The machine learning models were implemented in a user-friendly tool, which can be used for design purposes.

## 1. Introduction

There are ever-increasing demands to improve the durability and the entire life performance of steel structures. In this context, stainless steel has recently emerged as a highly desirable option for structural applications owing to its distinctive characteristics which include outstanding corrosion resistance, long lifespan and recyclability (Rabi et al., 2022a). Moreover, stainless steel offers an attractive aesthetic appearance with excellent mechanical strength, significant strain hardening and great ductility. Although stainless steel has a relatively higher initial cost, it becomes a more competitive and efficient alternative design option than carbon steel, given the reduction in costs

associated with regular inspections and maintenance and rehabilitation works (Rabi et al., 2022b). The use of stainless steel circular hollow sections (CHS) has widely increased in recent years, mainly due to its exceptional aesthetic appearance and excellence performance in compression, bi-axial bending resistance and torsional resistance. They have been used in a wide range of structural members such as columns, beams, arches, trusses, and wind turbine towers. This paper concerns the behaviour of stainless steel CHS.

Stainless steel has a different constitutive behaviour than carbon steel, exhibiting a continuous rounded response from an early stage with an undefined yield point, while exhibiting substantial strain hardening and ductility. Conversely, carbon steel exhibits a linear relationship

\* Corresponding author.

E-mail address: [Rabee.Shamass@brunel.ac.uk](mailto:Rabee.Shamass@brunel.ac.uk) (R. Shamass).

<https://doi.org/10.1016/j.engappai.2024.107952>

Received 31 August 2023; Received in revised form 17 January 2024; Accepted 19 January 2024

Available online 15 February 2024

0952-1976/© 2024 The Authors. Published by Elsevier Ltd. This is an open access article under the CC BY license (<http://creativecommons.org/licenses/by/4.0/>).

within the elastic range with a well-defined yield point followed by a moderate degree of strain hardening (Rabi et al., 2020). Thus, the typical 0.2 % proof stress is typically adopted to determine the yield stress. Despite the difference in the material stress-strain behavior, various existing design standards (EN, 1993, 2006; SEI/ASCE 8-02, 2002; AS/NZS 4673, 2001) limit the load carrying capacity of stainless steel to the 0.2 % proof stress, neglecting the pronounced strain hardening and large ductility. Given the high initial costs of stainless steel, it is imperative to develop a more accurate design approach, reflecting the actual material response.

The rapid advancement of computerized artificial intelligence has provided an efficient and reliable approach for solving complex engineering problems (Meng et al., 2023a, 2023b; Aye et al., 2019; Xu et al., 2024; Anosri et al., 2023). Machine Learning methods have been employed in different structural applications through the development of design formulas that can account for various influential parameters including damage detection, reliability analysis and capacity prediction of structural elements. Artificial Neural Network (ANN) and Support Vector Machine (SVM) have been widely used in various applications including structures, energy, medicine (Ashraf et al., 2021; Huang et al., 2017). They have been recognized in structural applications for accurately predicting the behavior of structural elements (Malami et al., 2021; Golafshani et al., 2012; Kari et al., 2018a; Nguyen et al., 2021a; Rabi, 2023). ANN operates on schematic procedures that involve pattern recognition and prediction. There are three typical layers in the ANN including the input layer, hidden layer, and output layer. The hidden layer comprises of several weighted connections that interconnect the input and output parameters. Support Vector Machine Regression (SVR) contains a subset of training samples that are used for the determination of the SVR model. The key aspect of SVR is to determine an optimal hyper-plane that most accurately fits the training data while enabling a certain margin of error. Others machine learning methods are also introduced for predicting complex engineering problems such as Gene Expression Programming (GEP) and Regression Trees (RT). Both of these supervised machine learning algorithms have excellent ability to generate predictive models with sufficient level of accuracy. The typical architectural form of the GEP is composed of individual chromosomes that create an expression tree of multiple genes (Jweihan et al., 2023; Jweihan, 2023; Almomani et al., 2023). The RT Gradient Boosting Trees (GBT) is an ensemble algorithm comprising numerous base models or learners. Each base learner is an individual tree model constructed by training on a bootstrap sample from the training data. The process involves partitioning the feature space into a collection of regions and fitting a simple model for each region (Friedman, 2001, 2002)

A series of experimental tests on stainless steel stub columns and beams has been previously conducted on various sections including I-sections (Yuan et al., 2014; Yang et al., 2023; Saliba and Gardner, 2013), square and rectangular hollow sections (Zhou and Young, 2005; Theofanous and Gardner, 2010; Huang and Young, 2013; Shu et al., 2013; Afshan and Gardner, 2013a), angle sections (Kuwamura, 2003; Theofanous et al., 2015) and channel sections (Becque and Rasmussen, 2009; Rossi et al., 2010; Niu et al., 2014). A limited number of research focused on the stainless steel circular hollow sections (CHS) stub columns (Young and Hartono, 2002; Kiyamaz, 2005; Bardi and Kyriakides, 2006; Buchanan et al., 2018). Young and Hartono (2002) examined the behaviour of stainless steel circular hollow section (CHS) columns subjected to compression loading. Various column length was considered to develop local and global buckling failure. A comparison of the ultimate test strengths and corresponding international design values was presented. The results indicated conservative predictions of the tested specimen. Kiyamaz (2005) conducted a series of experimental tests on the stainless steel circular hollow sections subjected to bending using austenitic and duplex stainless steel. Over-conservative predictions of the ultimate capacity were reported. Bardi and Kyriakides (2006) carried fifteen stainless steel stub columns using CHS sections. The specimens were tested in pure compression. More recently, Buchanan et al.

(2018) tested a total of 47 stainless steel CHS columns and conducted a large parametric study. The tests included austenitic, duplex and ferritic grades. It was observed that the current design approach given in the Eurocode 3 provided conservative predictions of the ultimate capacity of the section. These studies revealed that the codified capacity predictions tend to be very conservative when compared with the corresponding experimental results. Some research studies have proposed an analytical approach to improve the efficiency of the design predictions of stainless-steel sections such as the continuous strength method (Ashraf et al., 2008; Afshan and Gardner, 2013b; Buchanan et al., 2016; Liew and Gardner, 2015; Rabi et al., 2019, 2021; Shamass and Cashell, 2019).

Machine learning methods have been widely implemented to study the behavior of various structural steel elements including beam-columns (Toffolon et al., 2021; Müller et al., 2022; Müller and Taras, 2022a, 2022b; Rabi et al., 2023a), beams (Dai et al., 2022a; Dai et al., 2022b; Fang et al., 2022; Fang et al., 2021a; Fang et al., 2021b; Güneysisi et al., 2014; D'Aniello et al., 2015), plates (Tohidi and Sharifi, 2016; Sharifi et al., 2016; Pu and Mesbahi, 2006), cellular and castellated beam (Hosseinpour et al., 2020; Limbachiya and Shamass, 2021; Ferreira et al., 2022; Tohidi and Sharifi, 2015; Nguyen et al., 2020; Gholizadeh et al., 2011) and columns (Dai et al., 2022b; Fang et al., 2021a, 2022). However, there is very limited research on the behavior of stainless steel beams (Nguyen et al., 2021b; Du et al., 2017; Zarringol et al., 2021; Graciano et al., 2021; Dissanayake et al., 2022) and columns (Xu et al., 2021). Therefore, the present paper aims to predict the cross-section capacity of a stainless steel CHS column based on the most popular machine learning methods, particularly the Artificial Neural Network (ANN), the Support Vector Machine Regression (SVR), Gene Expression Programming (GEP), and Decision Trees for Regression (DTR). A finite element (FE) model was developed and validated using available test data. An extensive parametric study with a total of 1524 data points was conducted to train and validate the ANN, SVR, GEP and DTR models. Moreover, the accuracy of the current design rules in the prEN 1993-1-4:2006 (EN, 1993, 2006) is assessed through a comparative study with the results obtained from the FE model and various ML models.

## 2. Eurocode 3 design rules

In this section, the current design rules given in the Eurocode 3 prEN 1993-1-4:2006 (EN, 1993, 2006) for stainless steel CHS stub column are examined. It is worth noting that the current design rules in prEN 1993-1-4:2006 (EN, 1993, 2006) for structural stainless steel CHS members under compression load adopts relatively the same design provisions given in prEN 1993-1-1:2020 (European Committee for Standardization, 2020) for members made from carbon steel. According to Eurocode 3, the cross-sections are classified into four different classes based on the susceptibility to local buckling and deformation capacity, under a given load. Class 1 and 2 cross-sections can reach the full plastic sectional resistance, whereas class 3 cross-sections only reach the elastic sectional resistance and do not attain the full plastic resistance owing to inelastic local buckling failure. The most sensitive cross-sections to local buckling are classified as class 4 cross-sections, which fail prior to reaching the elastic sectional resistance. A specified slenderness limit for stainless steel CHS ( $D/te^2$ ) is given in Eurocode 3 (EN, 1993, 2006) for each class, in which  $D$  and  $t$  are the outer diameter and the thickness of the member, respectively, and  $\varepsilon$  is a parameter defined as given Eq. (1) for stainless steel members. These limits for class 1 to 3 cross-sections are set to be 50, 70, 90, respectively. The upper bound of the slenderness limit for class 4 cross-sections is 240.

The designed cross-sectional capacity is calculated from Eq. (2), where  $N_{Ed}$  and  $N_{c,Rd}$  represent the design ultimate compression load and the cross-sectional resistances to compression, respectively,  $\gamma_{M0}$  is the partial safety factor taken as 1.1 for stainless steel members. For class 1 to 3 cross-sections,  $N_{c,Rd}$  is equal to the product of the 0.2 % proof stress ( $\sigma_{0.2}$ ) and the gross cross-sectional area ( $A$ ). Where on other hand for

**Table 1**  
Geometric properties of models tested by Zhao et al. (2016a)

Cross-section	L (mm)	D (mm)	t (mm)
CHS 60.5 x 2.8	200.2	60.40	2.78
CHS 76.3 x 3.0	240.0	76.42	2.98
CHS 114.3 x 3.0	360.1	114.52	2.89
CHS 139.4 x 3.0	434.8	139.80	2.92

**Table 2**  
Physical properties of models tested by Zhao et al. (2016a)

Cross-section	$E_0$ (GPa)	$\sigma_{0.2}$ (MPa)	$\sigma_u$ (MPa)	$\epsilon_{tu}$ (%)	R-O coefficient	
					n	$n'_{0.2,u}$
CHS 60.5 x 2.8	190	355	780	47	5.3	1.9
CHS 76.3 x 3.0	195	302	784	48	7.3	1.9
CHS 114.3 x 3.0	187	290	799	45	7.8	1.6
CHS 139.4 x 3.0	188	323	757	52	4.9	1.8

class 4 sections, the effective cross-sectional area ( $A_{eff}$ ) is implemented instead of the gross cross-sectional and is calculated from Eq. (3).

$$\epsilon = \sqrt{\left(\frac{235}{f_y}\right) \left(\frac{E}{210000}\right)} \quad (01)$$

$$\frac{N_{Ed}}{N_{c,Rd}/\gamma_{M0}} \leq 1.0 \quad (02)$$

$$A_{eff} = A \sqrt{\frac{90\epsilon^2}{D/t}} \quad (03)$$

### 3. Finite element method: Validation and parametric study

For development of the numerical model, Abaqus software (Dassault Systèmes Simulia, 2016) is used. Processing is carried out in two steps, considering buckling and post-buckling analyses. The first buckling mode is then used as the initial geometric imperfection. In this context, the initial geometric imperfection is applied in the post buckling analysis using the \*IMPERFECTION command, by a factor equal to  $t/100$ . Residual stresses were not considered, as reported in Zhao et al., 2016a, 2016b.

#### 3.1. Tests

Three different types of cross section, length, diameter, and thickness are considered, as shown in Table 1. In total, four stub columns are validated against the finite element model.

#### 3.2. Material

The constitutive model used for the validation study is presented in (Rasmussen, 2003), according to Eqs. 04–08. Table 2 presents the physical properties of the material. The implementation of the stress-strain relationship must be done considering true stresses and true plastic strains.

$$\epsilon = \begin{cases} \frac{\sigma}{E_0} + 0.002 \left(\frac{\sigma}{\sigma_{0.2}}\right)^n, & \sigma < \sigma_{0.2} \\ \left(\frac{\sigma - \sigma_{0.2}}{E_{0.2}}\right) + \left(\epsilon_{tu} - \frac{\sigma_u - \sigma_{0.2}}{E_{0.2}} - \epsilon_{t0.2}\right) \left(\frac{\sigma - \sigma_{0.2}}{\sigma_u - \sigma_{0.2}}\right)^{n'_{0.2,u}} + \epsilon_{t0.2}, & \sigma \geq \sigma_{0.2} \end{cases} \quad (04)$$

$$\epsilon_{t0.2} = \frac{\sigma_{0.2}}{E_0} + 0.002 \quad (05)$$

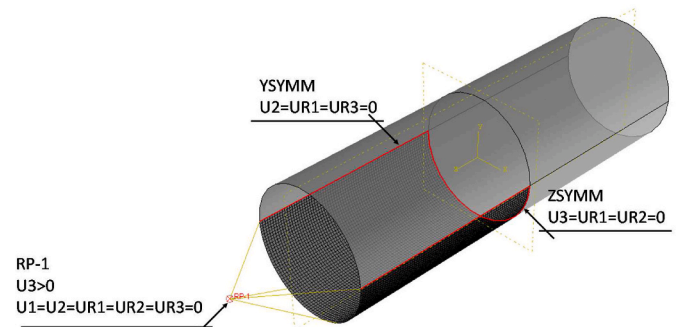


Fig. 1. Boundary conditions.

$$E_{0.2} = \frac{E_0}{1 + 0.002n \frac{E_0}{\sigma_{0.2}}} \quad (06)$$

$$\sigma_{True} = \sigma_{Eng} (1 + \epsilon_{Eng}) \quad (07)$$

$$\epsilon_{True}^p = \ln(1 + \epsilon_{Eng}) - \frac{\sigma_{True}}{E_0} \quad (08)$$

#### 3.3. Boundary conditions and discretization

In the numerical model, two planes of symmetry were adopted, aiming at reducing the computational cost (Fig. 1). This modeling technique has been adopted in several research papers (Zhao et al., 2016a, 2016b, 2016c; Meng et al., 2020). The discretization of the stub columns was performed using the S4R element available in the Abaqus software library (Dassault Systèmes Simulia, 2016). It is a quadrilateral element with four nodes and reduced integration, a factor that reduces processing time. S4R has six degrees of freedom per node - three rotations and three translations. The dimension of the elements was taken equal to the thickness ( $t$ ) of the stub columns (Zhao et al., 2016a).

#### 3.4. Validation results

Fig. 2 shows the validation results against tests performed by Zhao et al. (2016a). According to this reference, all the stub columns failed by inelastic local buckling with an elephant foot pattern. This failure mode was also a characteristic of the developed numerical models.

It can be observed from Table 3 that the percentage differences in the ultimate bearing capacity between the FE model and test results vary between 6 % and 10 % (on the conservative side) with an average of 5 % and coefficient of variation of 0.14 %. It can be concluded that the FE model adopted is capable of providing an accurate prediction of the behaviour of stainless steel stub columns and will be used for further parametric studies to predict the load capacity.

#### 3.5. Parametric study

In the parametric study, six diameters (60, 90, 120, 180, 240, and 300 mm), seven thicknesses (2, 3, 4, 5, 6, 7, and 8 mm) and eight length values (180, 270, 360, 450, 600, 900, 1200, and 1500 mm) were considered. The diameter-to-thickness ( $D/t$ ) ratio ranges between 7.5 and 150 and the length-to-diameter ( $L/D$ ) ratio ranges between 0.6 and 25. In total, five stainless steels were considered, and the mechanical properties are shown in Table 4. Python scripting is used to carry out parametric study and post-process the results.

### 4. Machine learning algorithms

In this paper, four machine learning algorithms, namely Support Vector Machine Regression, Artificial Neural Network, Gene Expression

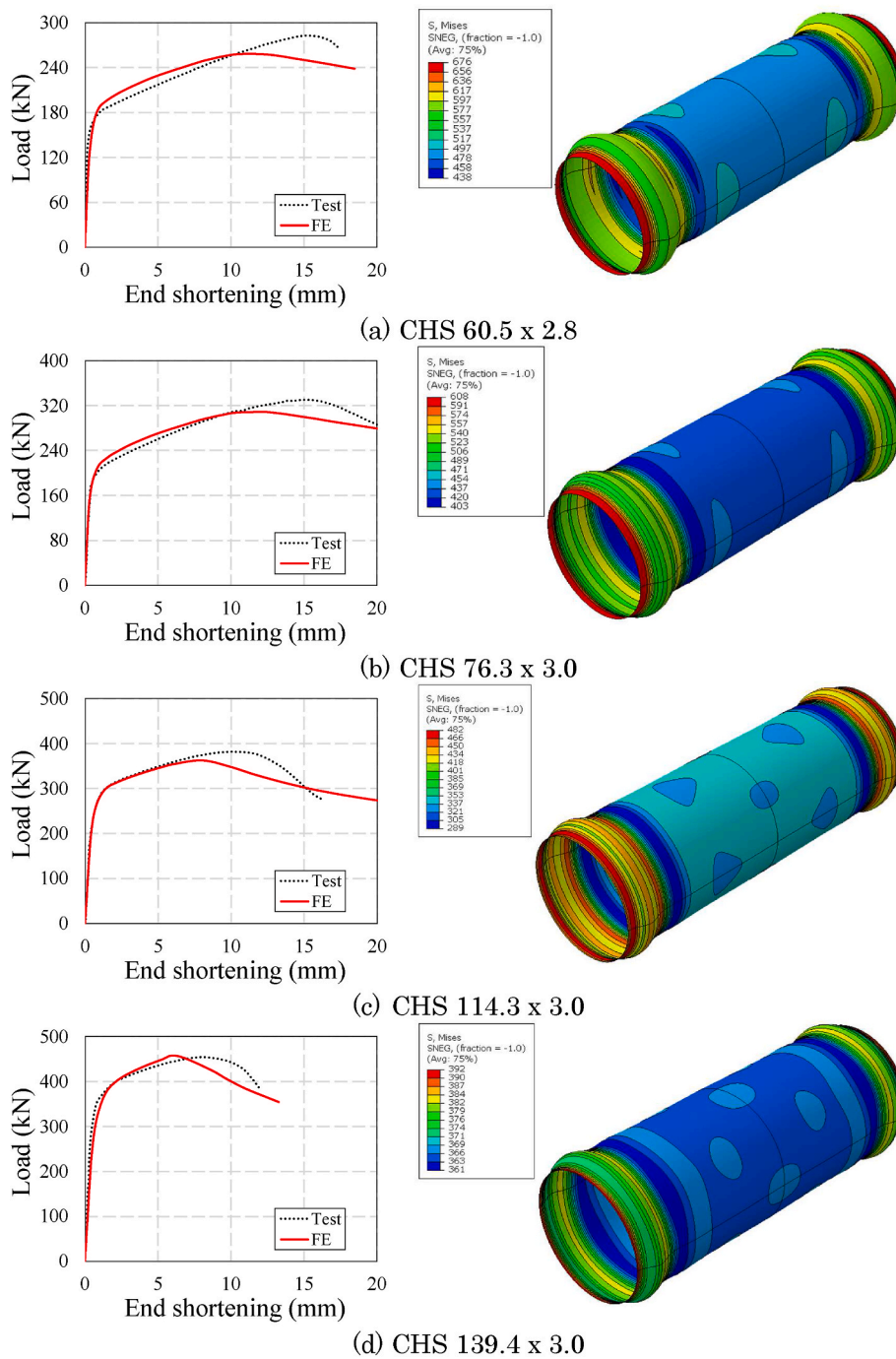


Fig. 2. Finite element method vs. tests by load-end shortening relationship.

Table 3  
Summary of validation results.

Cross-section	$N_{it}$ (kN)	$N_{FE}$ (kN)	$N_{it}/N_{FE}$
CHS 60.5 x 2.8	283.6	258.1	1.10
CHS 76.3 x 3.0	329.5	308.5	1.07
CHS 114.3 x 3.0	382.7	362.6	1.06
CHS 139.4 x 3.0	456.3	457.5	1.00
		<b>Average</b>	1.05
		<b>S. D.</b>	0.04
		<b>Var.</b>	0.14 %

Programming and Decision Trees for Regression will be used to predict the ultimate load capacity of the stainless steel columns. The data generated from the parametric study will be used to test, train, and validate the machine learning methods. It is worth pointing out that linear, polynomial, Radial Basis Function RBF and sigmoid kernel functions are tested and discussed when using SVM. Six input variables were chosen for the machine learning, namely, the outer diameter ( $D$ ), the thickness ( $t$ ), the length ( $L$ ), the yield strength at 0.2 % offset ( $f_{0.2}$ ), the ultimate strength ( $f_u$ ), and the Romberg-Osgood exponent ( $n$ ). The output variable of the machine learning is the cross-section resistance of the CHS stainless steel stub columns ( $N_{it}$ ).

**Table 4**  
Physical properties of stainless steel used for the parametric study.

Grade	$E_0$ (GPa)	$\sigma_{0.2}$ (MPa)	$\sigma_u$ (MPa)	$\epsilon_{tu}$ (%)	R-O coefficient	
					n	n' <sub>0.2,u</sub>
Austenitic (Sharifi et al., 2016)	190	355	780	47	5.3	1.9
Austenitic (Sharifi et al., 2016)	187	290	799	45	7.8	1.6
Austenitic (Sharifi et al., 2016)	188	323	757	52	4.9	1.8
Austenitic (Pu and Mesbahi, 2006)	195	302	784	85	7.3	1.9
Duplex (Pu and Mesbahi, 2006)	199	519	728	65	5.3	3.7
Ferritic (Pu and Mesbahi, 2006)	190	466	515	68	6.6	7.6

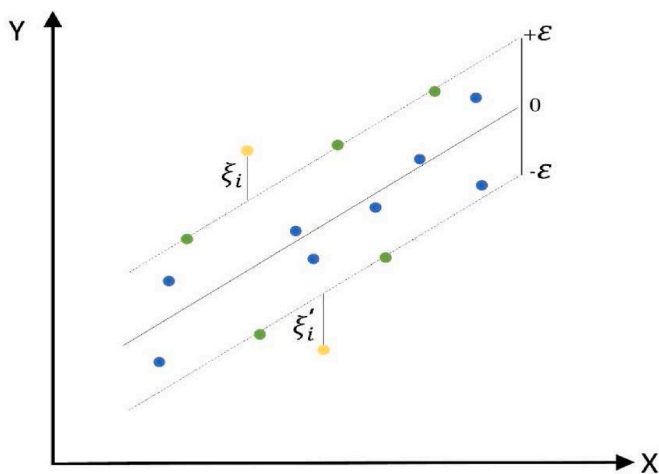


**Fig. 3.**  $\epsilon$ -insensitive tube for SVR, with green points correspond to margin SVs, and yellow points represent data with non-zero slack variables.

#### 4.1. Support Vector Machines

##### 4.1.1. Theoretical background

Support Vector Machine is a supervised machine learning method originally created in the 90s by Vapnik, 1995, 1998, 1999 and has gained significant popularity over the last decades due to its reliability and effectiveness (Kari et al., 2018b; Nguyen et al., 2021c). SVM was originally created for classification problems and is known as Support Vector Classification (SVC) and has been then extended to regression tasks and referred to as Support Vector Regression (SVR). The key aspect of SVR is to determine an optimal hyper-plane that most accurately fits the training data while enabling a certain margin of error, denoted  $\epsilon$ , as indicated Fig. 3. Predictions that fall within the  $\epsilon$ -insensitive tube are assumed to have acceptable deviations from the target values, however, any deviation greater than  $\epsilon$  are penalized (Awad et al., 2015). Support vectors (SVs) are a subset of training samples that have a significant impact in determining the SVR model as they directly influence its accuracy and generalization capability. While the computational complexity of ANN model is influenced by the number of layers, neurons per layer and the type of activation functions used, the complexity of SVR depends primarily on the number of support vectors. This means that, the more support vectors there are, the more computationally challenging the SVR model becomes (Lin and Lin, 2003).

In many practical applications, the relationship between input and output is often not simply linear in the original input space. For this purpose, SVR relies on the concept of the kernel trick to map the input

data into a higher dimensional space where nonlinear relationship in the original input space can be captured by a linear decision surface (i.e., hyper-plane). This can be achieved using kernel function that enables SVR to deal with complex non-linear data and make accurate predictions. Indeed, the right choice of kernel function is also very important for an effective model performance. A brief overview of the theoretical background of the SVR is presented in this paper. Further detailed descriptions are found in (Smola and Schölkopf, 2004; Fletcher, 2009).

Considering a set of training data with  $N$  input  $x_1, \dots, x_N$  and corresponding observed values  $y_1, \dots, y_N$ , where  $x_i \in \mathbb{R}^n$  and  $y_i \in \mathbb{R}$ , with  $i = (1, 2, \dots, N)$ . The mathematical intuition behind SVR is to find a prediction model with the following form:

$$f(x) = w^T \phi(x) + b \quad (9)$$

While minimizing the following objective function:

$$\min_{w,b} \frac{1}{2} \|w\|^2 \quad (10)$$

$$\text{Subjected to: } \begin{cases} y_i - w^T \phi(x_i) - b \leq \epsilon \\ w^T \phi(x_i) + b - y_i \leq \epsilon \end{cases}$$

where  $w$  and  $b$  represent the regression function coefficients, and  $\phi(x)$  represents the mapping function of the input data to a higher-dimensional input space.

In certain cases, there is no optimal solution for the optimization problem defined by Eq. (10), because the imposed constraints are very strict, which require that all observation must lie inside the  $\epsilon$ -insensitive tube as illustrated in Fig. 3. Hence, any violation outside the margin leads to its infeasibility (Smola and Schölkopf, 2004; Fletcher, 2009; Cortes and Vapnik, 1995). In order to address this issue, the concept of soft margin was introduced by Cortes and Vapnik (1995), which enables to tolerate and deal with some degree of error in the model, this is done by incorporating slack variables  $\xi_i, \xi'_i$ , which represent the upper and lower training deviations, respectively, outside  $\epsilon$ -insensitive tube, as shown in Fig. 3. Hence, the optimization problem can be reformulated as follows:

$$\min_{w,b,\xi_i,\xi'_i} \frac{1}{2} \|w\|^2 + C \sum_{i=1}^N (\xi_i + \xi'_i) \quad (11)$$

$$\text{Subjected to: } \begin{cases} y_i - w^T \phi(x_i) - b \leq \epsilon + \xi_i \\ w^T \phi(x_i) + b - y_i \leq \epsilon + \xi'_i \\ \xi_i, \xi'_i \geq 0; i = 1, 2, 3, \dots, N \end{cases}$$

where  $C$  represents the cost factor and is a positive parameter that determines the trade-off between the flatness of the regression function  $f$  and the error tolerance (Smola and Schölkopf, 2004; Fletcher, 2009), and  $\epsilon$  is the error tolerance. Both  $C$  and  $\epsilon$  are hyper-parameters that need to be optimized during training process to ensure a good performance of SVR model.

Then, the optimization problem can be reformulated by introducing Lagrange multipliers  $\alpha_i$  and  $\alpha'_i$  as follows:

$$\max_{\alpha_i, \alpha'_i} \sum_{i=1}^N y_i (\alpha_i - \alpha'_i) - \epsilon \sum_{i=1}^N (\alpha_i + \alpha'_i) - \frac{1}{2} \sum_{i,j=1}^N (\alpha_i - \alpha'_i) (\alpha_j - \alpha'_j) \phi(x_i)^T \phi(x_j) \quad (12)$$

$$\text{Subjected to: } \sum_{i=1}^N (\alpha_i - \alpha'_i) = 0 \quad \alpha_i, \alpha'_i \in [0, C]; i = 1, 2, 3, \dots, N.$$

Therefore, the prediction model can be rewritten as:

$$f(x) = \sum_{i=1}^N (\alpha_i - \alpha'_i) \phi(x_i)^T \cdot \phi(x) + b \quad (13)$$

where;  $w = \sum_{i=1}^N (\alpha_i - \alpha'_i) \phi(x_i)^T$ .

The solution for Lagrange multiplier coefficients  $(\alpha_i - \alpha'_i)$  may include both zero and non-zero values. The non-null terms correspond to the SVs and only these latter contribute to the final regression function.

**Table 5**  
Common kernels functions (Karatzoglou et al., 2006).

Kernel Function	Mathematical Formula	Hyper-parameters
Linear	$K(x_k, x) = x_k^T x$	$C$ and $\epsilon$
Polynomial	$K(x_k, x) = (x_k^T x + r)^d$	$C$ , $d$ , $r$ and $\epsilon$
RBF	$K(x_k, x) = \exp(-\gamma \ x_k - x\ ^2)$	$C$ , $\gamma$ and $\epsilon$
Sigmoid	$K(x_k, x) = \tanh(\gamma x_k^T x + r)$	$C$ , $\gamma$ , $r$ and $\epsilon$

$C$ : cost;  $\epsilon$ : error tolerance;  $\gamma$ : coefficient;  $r$ : offset;  $d$ : degree.

Hence, Eq. (13), can be re-expressed as:

$$f(x) = \sum_{k=1}^{nSVs} (\alpha_k - \alpha_k^*) K(x_k, x) + b \quad (14)$$

In this equation,  $x$  represents the input vector,  $x_k$  denotes the support vectors,  $nSVs$  is the number of support vectors,  $b$  is the bias, and  $K(x_k, x) = \phi(x_k)^T \cdot \phi(x)$  represents the kernel function. The most used kernels are linear, polynomial, the radial basis function (RBF) kernel, and sigmoid kernel, of which the mathematical expressions are reported in Table 5 together with the corresponding hyper-parameters that should be optimized. Accordingly, this research paper aims to predict the cross-section resistance ( $N_u$ ) of CHS stainless steel stub columns using  $\epsilon$ -SVR with aforementioned kernels.

#### 4.1.2. Data pre-processing

In this paper, 1524 datasets obtained from the parametric study are used to train, validate and test the performance of SVR model using *fitrsvm* function available in statistics and machine learning toolbox in MATLAB 2020a (MATLAB and Statistics Toolbox Release, 2019). Each data pair consists of six input variables, ( $D$ ), ( $t$ ), ( $L$ ), ( $f_{0.2}$ ) ( $f_u$ ), and ( $n$ ) while the output is the cross-section resistance ( $N_u$ ). Since these variables have different units and quantity limits as shown in Table 6, the input and output are normalized to ensure that all values are scaled in a consistent interval range, between 0 and 1. For this purpose, the following equation is used:

$$x_i^n = \frac{x_i - x_i^{min}}{x_i^{max} - x_i^{min}} \quad (15)$$

where  $x_i$  and  $x_i^n$  denote the original and normalized values of the  $i$ -th component in the input vector,  $x_i^{min}$  and  $x_i^{max}$  represent the minimum and maximum values, respectively, for the  $i$ -th component of the input vector  $x_i$  before normalization.

It should be noted that 70 % of datasets are devoted for training the SVR models in which the model is evaluated in response to statistical metrics. Furthermore, 15 % is reserved for validation purposes, where the performance and generalization capacity of the SVR models is examined, and the remaining 15 % is used for testing unseen dataset by the model.

#### 4.1.3. Performance evaluation

In order to examine the performance and accuracy of SVR models, statistical metrics such as coefficient of determination ( $R^2$ ), the Root Mean Square Error ( $RMSE$ ) and the Mean Absolute Error ( $MAE$ ) are used and are expressed by Eqs. (16a), (16b), and (16c), respectively. These measures enable to make a direct comparison between the predicted and actual outputs.

**Table 6**  
Range of the input and output parameters.

	$D$ (mm)	$t$ (mm)	$L$ (mm)	$f_{0.2}$ (MPa)	$f_u$ (MPa)	$n$	$N_u$ (kN)
Lower limit	60	2	180	290	515	4.9	112.07
Upper limit	300	8	1500	519	799	7.8	4430.70

$$R^2 = 1 - \frac{\sum_{i=1}^m (y_i - \hat{y}_i)^2}{\sum_{i=1}^m (y_i - \bar{y})^2} \quad (16a)$$

$$RMSE = \sqrt{\frac{1}{m} \sum_{i=1}^m (y_i - \hat{y}_i)^2} \quad (16b)$$

$$MAE = \frac{1}{m} \sum_{i=1}^m |y_i - \hat{y}_i| \quad (16c)$$

where,  $y_i$  and  $\hat{y}_i$  denote the  $i$ th actual and predicted output respectively,  $\bar{y}$  represent the average of  $y_i$  and  $m$  is the number of data point. To achieve excellent SVR model accuracy, the value of ( $R^2$ ) should be close to 1, and ( $RMSE$ ) and ( $MAE$ ) must be minimal.

On the other hand, the correlation between input variables and the output is examined using Pearson's approach (Pearson, 1895). This analysis gives insights into the strength and direction of linear inter-dependence between input variables, as well as their impact on the output parameter. Pearson's correlation coefficient ( $\rho$ ) can be calculated using the following expression for two variables  $X$  and  $Y$ :

$$\rho = \frac{\sum_i (X_i - \bar{X})(Y_i - \bar{Y})}{\sqrt{\sum_i (X_i - \bar{X})^2 \sum_i (Y_i - \bar{Y})^2}} \quad (17)$$

in which,  $X_i$  and  $Y_i$  are the values of the variable  $X$  and  $Y$ , respectively, for  $i$ th observation.  $\bar{X}$  and  $\bar{Y}$  are the average values of the variables  $X$  and  $Y$ , respectively. Pearson's correlation coefficient ranges between  $-1$  and  $1$ .  $\rho$  equals to 1 (or alternatively,  $-1$ ) indicates a strong positive (or negative) correlation, which mean as  $X$  increases,  $Y$  increases (or decreases). When  $\rho$  is 0, indicates no correlation between the two variables  $X$  and  $Y$ .

#### 4.1.4. Grid search method

To find the optimal combination of the hyper-parameters specified in Table 5 for the SVR models, considering different kernel types, grid search technique with cross validation is used to tune these hyper-parameters. Although this technique is exhaustive and computationally time-consuming, especially if the search range is large, it is widely used in literature due to its high accuracy (Syarif et al., 2016). To reduce the computational time, as recommended in the practical guide (Hsu

**Table 7**  
Hyper-parameters range.

	Kernel type	Min	Max	Step size	Type	Scale
$C$	linear, polynomial, RBF, sigmoid	$2^{-5}$	$2^{15}$	$1^{**}$	real	power
$\epsilon$	linear, polynomial, RBF, sigmoid	$2^{-15}$	$2^{-1}$	$1^{**}$	real	power
$\gamma$	RBF, sigmoid	$2^{-11}$	$2^3$	$1^{**}$	real	power
$d$	polynomial	1	10	1	integer	linear
$r^*$	polynomial, sigmoid	-	-	-	-	-

\* $r$  is set to 1,

\*\*the step is reduced to 0.25 in finer grid search.

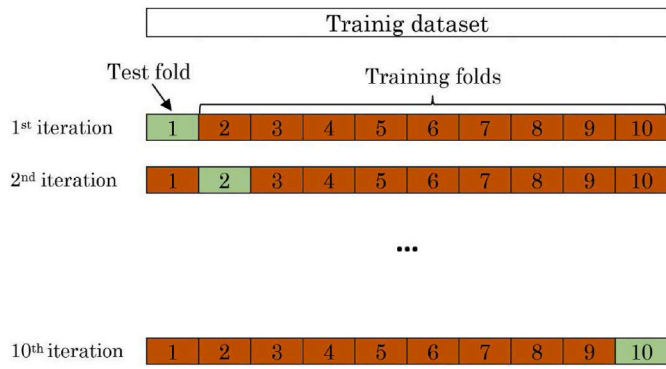


Fig. 4. A schematic representation of 10-fold cross-validation.

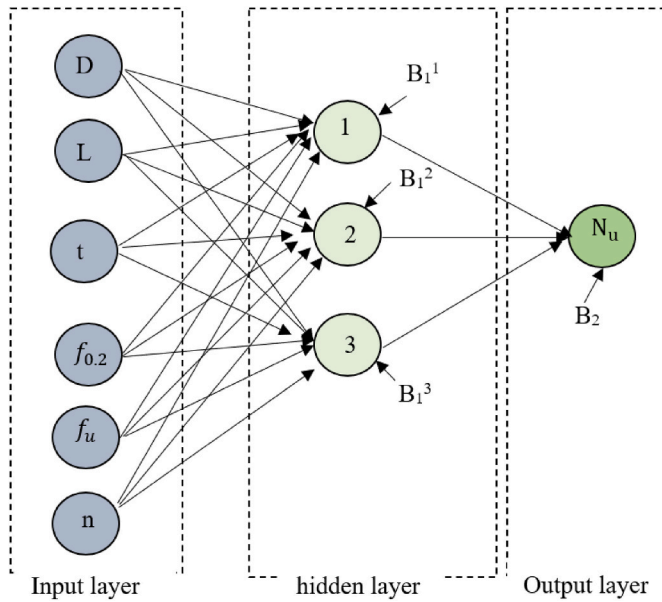


Fig. 5. ANN Model with 3 neurons in the hidden layer.

et al., 2003), this paper employs a two-step grid search approach. First, a coarse grid search was conducted, consisting of a wide range of values with a larger step size, this enables the identification of the interval where the optimal hyper-parameters are located. Then, a refined grid search was performed to find the best combination of the hyper-parameters, in which the step is reduced. Table 7 presents the considered range for the hyper-parameters for each SVR model's kernel type.

To prevent overfitting during the training process and ensure a more reliable performance estimate, the most commonly recommended technique is the 10-fold cross-validation (Sharifmousavi and Borhani, 2020). In the present study, this approach is implemented for each combination of hyper-parameters. The process involves dividing the data into 10 equal subsets, in each iteration one fold is used as a testing set while the remaining 9 folds serve as the training set, as schematically explained in Fig. 4. This process is repeated 10 times to ensure accurate results, in which the trained model is iteratively evaluated on the testing subset, and the average statistical metrics are recorded. Hence, the 10-fold cross-validation is performed for each combination across the specified range, and the combination of hyper-parameters that yields to a higher  $R^2$  value and minimal  $RMSE$  is selected as the best combination.

## 4.2. Artificial Neural Network

### 4.2.1. Neural network architecture

A Multi-Layer Perceptron Network (MLPN) that solved an input-output fitting problem with a two-layer feedforward neural network was used in this study to predict the ultimate resistance of CHS sections. Fig. 5 provides an example of a neural network architecture with three neurones. The overall aim of the neural network is to assign weights to the neurons in the hidden layer and bias values the hidden and output layer to determine connections between the input and output parameters. For this study, ANN models with 4, 6, 8 and 10 neurons in the hidden layer were created. The reason for this was firstly, an increase in the number of neurons in the hidden layer could result in overfitting of the data which would result in an inaccurate overview of the impact of input parameters. Secondly, as the number of neurons increases, the complexity of the equation increases, and the aim was to provide the simplest calculation to achieve a high level of accuracy.

### 4.2.2. Setting up Artificial Neural Network

The ANN initially divides the data into 3 categories. Training data (70 %) is used to train the network and adjust according to the errors, validation data (15 %) is used to measure network generalisation and stop the training when it stops improving and testing data (15 %) is data that has not been used in training or validation to independently assess the accuracy of the model (MATLAB and Statistics Toolbox Release, 2019). Due to the high level of accuracy for small to medium sized problems, the Levenberg-Marquardt backpropagation training algorithm was adopted (Nguyen et al., 2023; Tohidi and Sharifi, 2014; Sharifi et al., 2019; Rabi et al., 2023b).

All data variables were normalized using mapminmax method to get the data to range between -1 and 1. To do this, Eq. (18) was applied to all input and target parameters.

$$x_i^n = \frac{(y_{max} - y_{min})(x_i - x_i^{min})}{x_i^{max} - x_i^{min}} + y_{min} \quad (18)$$

Where  $x_i^n$  represents the normalized value,  $y_{min}$  and  $y_{max}$  represent the normalized data range of -1 and 1 respectively. Table 6 provides the minimum and maximum values of the parameters.

In total, 4 ANN models were produced. All had the same input and output parameters and the number of neurons ranged from 4 to 10. The choice of activation function involved experimentation and the characterization of the used data. Apicella et al. (2021) described a survey of trainable activation function in the neural network, highlighting general and unique properties of the recent and past approach. Eqs. (19) and (20) provide the Hyperbolic tangent sigmoid transfer function needed to predict the output parameter based normalized values (Gupta et al., 2019). This transfer function was chosen as it provided accurate predictions when it was used in other research studies (Jweihan et al., 2023; Rabi et al., 2023a; Limbachiya and Shamass, 2021; Ferreira et al., 2022). It is one of the most widely used transfer functions when constructing neural networks (Rabi et al., 2024).

$$O_s = B_1^s + \sum_{k=1}^r w_{k,l}^{ho} \left( \frac{2}{1 + e^{-2H_k}} - 1 \right) \quad (19)$$

$$H_k = B_2^k + \sum_{j=1}^q w_{j,k}^{ih} \cdot I_j \quad (20)$$

Where,  $O_s$  represents the normalized output value,  $q$  is the number of input parameters;  $r$  is the number of hidden neurons;  $s$  is the number of output parameters;  $B_1^s$  and  $B_2^k$  are the biases of sth output neuron and kth hidden neuron ( $H_k$ ), respectively;  $w_{j,k}^{ih}$  is the weights of the connection between  $I_j$  and  $H_k$ ;  $w_{k,l}^{oh}$  are the weights of the connection between  $H_k$  and  $O_s$ .

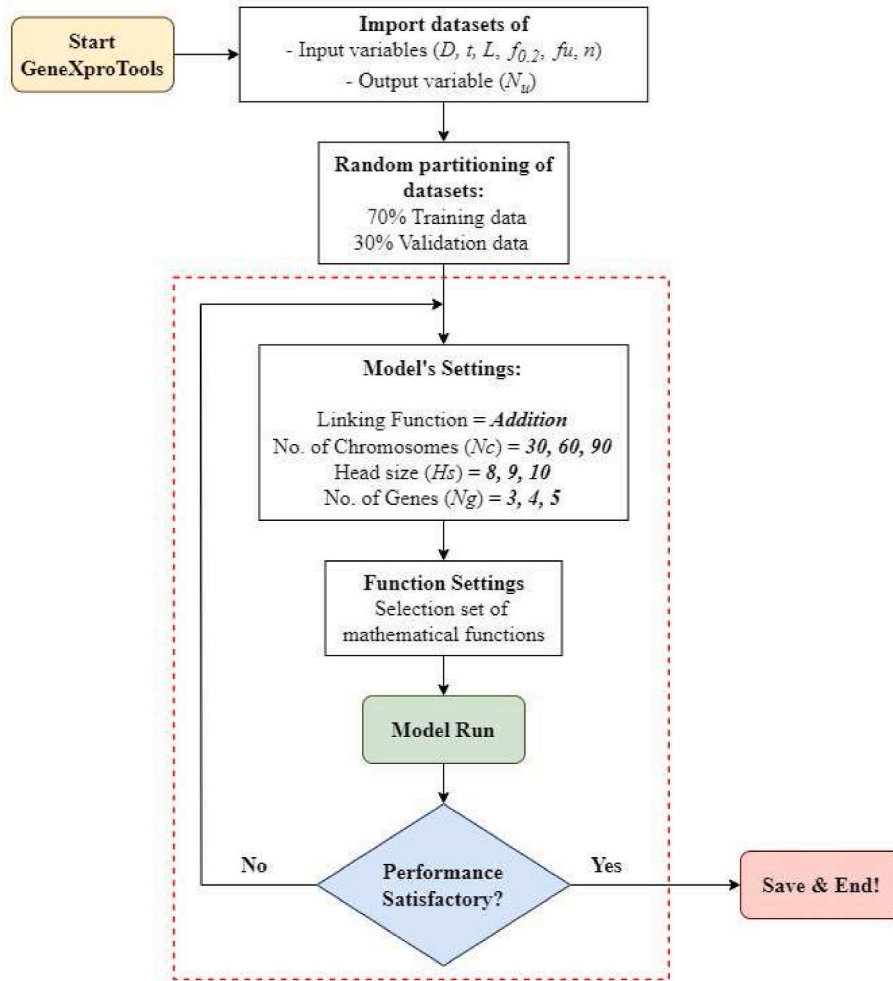


Fig. 6. Process of developing the GEP model.

#### 4.2.3. Assessing accuracy of neural network output

To assess the accuracy of the output the coefficient of determination ( $R^2$ ), Root Mean Square Error (RMSE) and Mean Absolute Error (MAE) were calculated using Eqs (16a), (16b) and (16c) respectively.

Since neural network models provide no explanation for how input signals contribute to the prediction process, they are commonly referred to as “black boxes” (Abellán-García, 2020). Therefore, to further assess the accuracy of the model, the impact of each input parameter was analysed using the Connection Weight Approach and Garson Algorithm (Garson, 1991). The Connection Weight Approach determines each input variable’s contribution and the direction of its relationship to the response variable with the use of raw connection weights (Iqbal et al., 2023). This results in the correct identification of variable contribution (Olden et al., 2004). The advantage of this approach is that it will determine whether the input parameter has a positive or negative impact on the output parameter. A positive impact will determine that an increase in the input parameter will increase the value of the output parameter and vice versa for a negative impact value. Eq. (21) provides the calculation process used in the connection weight approach in which  $Input_x$  represents the relative importance of the input variable,  $XY$  represents the connection weight between the input and hidden layer, and  $Hidden$  represents the connection weight between the hidden and output layer

$$Input_x = \sum_{Y=A}^E Hidden_{XY} \quad (21)$$

To further assess the accuracy, Garson’s Algorithm (Garson, 1991) was used to determine the impact of input parameters. Garson’s Algorithm assesses the relative significance of every input variable on the outcome, to partition the weight of the neural network link. The weights associated with hidden input and hidden output are divided, and the significant input variables are chosen based on the weights’ absolute values (Lau et al., 2023). By adopting both approaches, the study would be able to confidently determine the input parameters with significant impact. Eq. (22) provides the calculation used for Garson Algorithm (Olden et al., 2004). The subscripts  $k$ ,  $m$ , and  $n$  denote input, hidden, and output neurons, respectively, whereas the superscripts  $i$ ,  $h$ , and  $o$  denote input, hidden, and output layers, respectively.  $N_i$  and  $N_h$  are the numbers of neurons in the input and hidden layers, respectively;  $w$  represents connection weights.

$$I_j = \frac{\sum_{m=1}^{m=Nh} \left( \frac{w_{jm}^{ih} w_{mn}^{ho}}{\sum_{k=1}^{N_i} w_{km}^{ih}} \right)}{\sum_{k=1}^{k=Ni} \left[ \sum_{m=1}^{m=Nh} \left( \frac{w_{km}^{ih} w_{mn}^{ho}}{\sum_{k=1}^{N_i} w_{km}^{ih}} \right) \right]} \quad (22)$$

#### 4.3. Gene Expression Programming

GEP is one of the most popular machine learning (ML) tools that are

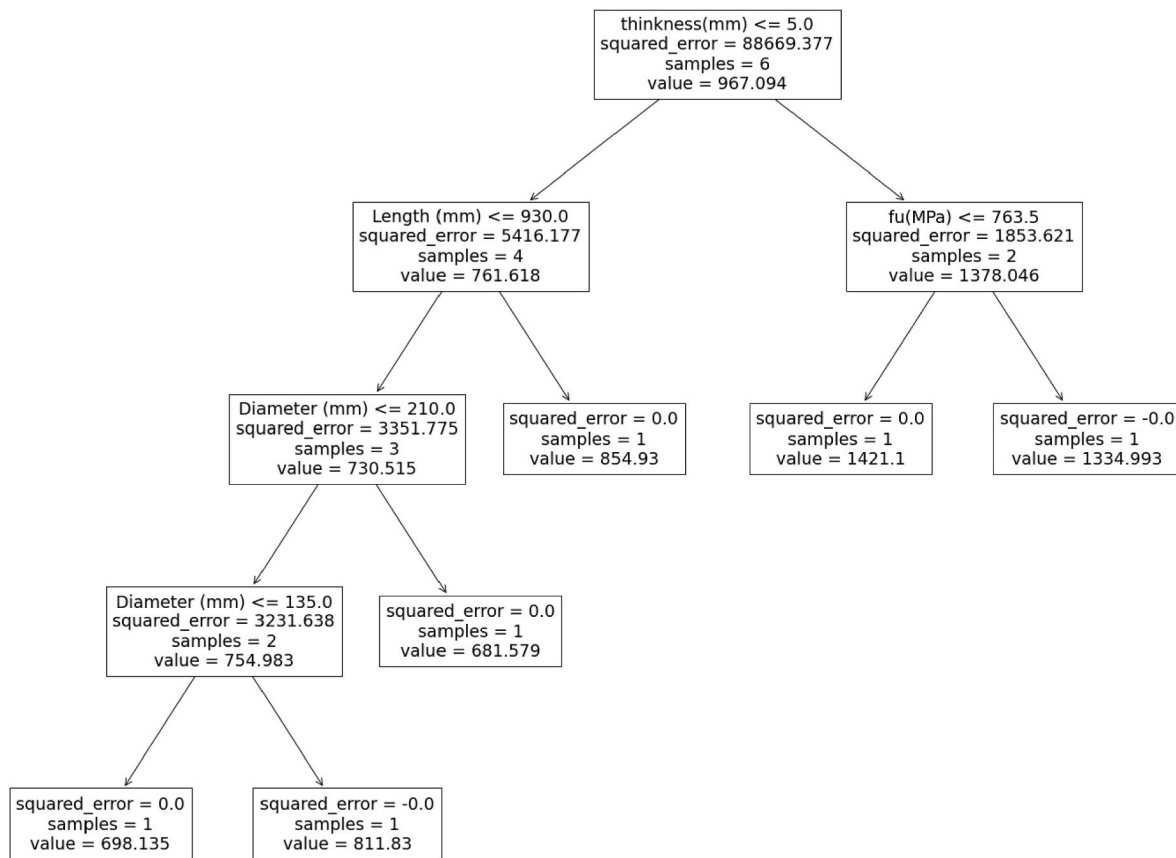


Fig. 7. Example of a regression tree.

widely harnessed by researchers for developing sophisticated models for predicting complex engineering problems with high accuracy (Jweihan, 2023; Almomani et al., 2023). The GEP outweighs other (ML) tools by means of its simplicity and superior ability to generate predictive models in the form of a direct mathematical equation. A GEP model is typically composed of individual chromosomes that create an expression tree (ET) of multiple genes. Basic mathematical functions like addition, multiplication, subtraction, and division are used as linking functions among these genes. Further information about the GEP approach can be found in Ferreira, 2001, 2002.

GeneXproTools software (Gene, 2000) has been utilized in this study to develop a GEP model. It is worth mentioning that developing a GEP model needs multiple trials to select the ideal parameters for the best-fitted predictive model. Previous studies indicated that the number of used chromosomes ( $N_C$ ) number of genes ( $N_g$ ), and head size ( $H_S$ ) of genes are crucial parameters in the software that control the accuracy and performance of a GEP model (Raheel et al., 2023; Khan et al., 2022). Thus, a sequential approach has been adopted in this study by interchanging ( $N_C$ ), ( $N_g$ ), and ( $H_S$ ) parameters to achieve the optimal GEP model. The ( $N_C$ ) were varied from 30 to 90, ( $N_g$ ) from 3 to 5, and  $H_S$  from 8 to 10, as illustrated in Fig. 6.

Similar to the previous models in this study, the GEP model considers the selected six input variables of the outer diameter ( $D$ ), the thickness ( $t$ ), the length ( $L$ ), the yield strength at 0.2 % offset ( $f_{0.2}$ ), the ultimate strength ( $f_u$ ), and the Romberg-Osgood exponent ( $n$ ) of the CHS stainless steel stub columns to predict the output variable of the columns' cross-section resistance ( $N_u$ ). The total database has been divided randomly by the GEP software into 70 % for training and 30 % for validation. Exploration trials on the software screened that the addition function is the most suitable linking function for developing a GEP model with high accuracy. The best-fitted and most accurate GEP model has been assigned after conducting many trials by changing the values of ( $N_C$ ,

( $H_S$ ) and ( $H_S$ ) parameters.

#### 4.4. Decision Trees for regression

Decision Trees for regression, or Regression Trees (RT) is a supervised machine learning algorithm which consists of finding the optimal way to split the dataset as to successfully reduce the variance of the sub datasets (Breiman, 2017). In each node of a RT, a Yes-or-No question is established to split the dataset, for example, "is the diameter greater than 63 mm?". By sequentially applying these nodes, a tree structure emerges that can be used to predict new points, as shown in Fig. 7.

The complexity of the tree is determined by its depth, the amount of vertical levels in the tree, and the number of leaves, which represent the end nodes without a decision. Fig. 7 shows a tree with 4 levels and 6 leaves. Also in Fig. 7, the top node asks the question "is the thickness less or equal than 5.0 mm?" where, at that stage, the dataset has a MSE of 88699.337. By answering that Yes-or-No question, the decision proceeds down the tree where further questions are answered. Note that the MSE reduces at each step until a node represents a single data point.

The optimal way to split the dataset is the one that minimised the MSE, which represents how the training values deviate from the nodal. To examine the performance of RTs, coefficient of determination  $R^2$  is determined. It is worth mentioning that the software used to perform the Decision Tree Regression algorithm was Python, specifically the scikit-learn library (Pedregosa et al., 2011).

## 5. Results and discussion

### 5.1. Eurocode 3

The results presented in this section are shown considering the type of stainless steel (Fig. 8), as well as the cross-section class (1-4),

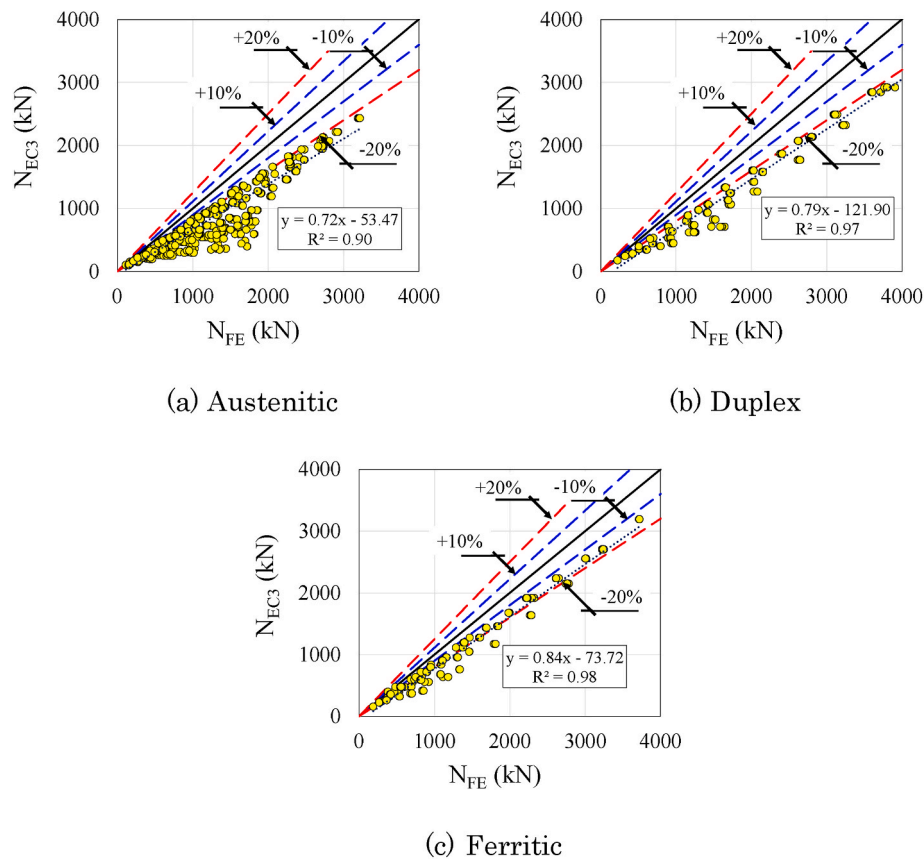


Fig. 8. Comparison of results considering the type of stainless steel.

according to Fig. (9). For austenitic, duplex, and ferritic stainless steels, 867, 333 and 324 finite element models were developed, respectively. For austenitic stainless steel (Fig. 8a), it was verified that all observations are in favor of safety ( $N_{EC3}/N_{FE} < 1.0$ ). The maximum and minimum relative errors ( $N_{EC3}/N_{FE} - 1$ ) were equal to -8 % and -77 %, respectively. For duplex stainless steel (Fig. 8b), the analysis was similar, all observations are in favor of safety ( $N_{EC3}/N_{FE} < 1.0$ ). However, for these models it was verified that the maximum and minimum relative errors were equal to -19 % and -57 %, respectively. On ferritic stainless steel (Fig. 8c), most of the analyses were also in favor of safety, with only one model being against safety. The values of relative errors were lower, the maximum and minimum relative errors were equal to 4 % and -51 %, respectively. These results showed that the calculation model presented by EC3 underestimates the cross-section resistance of a CHS stainless steel stub column. Table 8 presents the statistical analysis values.

The same comparative analysis performed previously can be done considering the class of the cross-section, as can be seen in the Fig. 9a, b and c. Similar to the previous analysis, the EC3 provides conservative predictions compared with corresponding numerical counterparts. The maximum and minimum relative errors ( $N_{EC3}/N_{FE} - 1$ ) were 4.5 % and -76.9 % for class 1 and 2, -13.4 % and -23.4 % for class 3 and -14.9 % and -53.4 % for class 4, respectively. The values of the statistical analyses are presented in Table 9.

## 5.2. Prediction-based support Vector Machines regression

The correlation between the six input variables, namely ( $D$ ), ( $t$ ), ( $L$ ), ( $f_{0.2}$ ), ( $f_u$ ), and ( $n$ ) employed in the SVR models as well as with the output ( $N_u$ ) is depicted in Fig. 10. It can be observed from the Pearson's correlation matrix, there is no linear correlation between some input parameters such as ( $D$ ) and ( $L$ ), ( $D$ ) and ( $f_u$ ), and ( $t$ ) and ( $n$ ), while a weak linear correlation is shown between some inputs such as ( $D$ ) and

( $f_{0.2}$ ), and ( $D$ ) and ( $t$ ) with correlation coefficients of  $-0.02$  and  $0.05$ , respectively. Furthermore, according to the present dataset, a strong negative correlation is observed between ( $f_u$ ) and ( $f_{0.2}$ ), and ( $f_{0.2}$ ) and ( $n$ ) with correlation coefficients of  $-0.6$  and  $-0.5$ , respectively. This could be attributed to the significant strain hardening and great ductility of stainless steel. On the other hand, a correlation coefficient of  $0.74$  between ( $N_u$ ) and ( $t$ ), and a correlation coefficient of  $0.58$  between ( $N_u$ ) and ( $D$ ), indicating a high linear relationship and influence between these input variables and the output. However, a low correlation coefficient between ( $N_u$ ) and ( $L$ ) as well as between ( $N_u$ ) and ( $f_u$ ), ( $N_u$ ) and ( $n$ ) meaning a weak linear correlation and minimal impact on the output. There is therefore a complex non-linear relationship between the cross-section resistance and the considered input variables, which is hard to express using a simple empirical equation.

As stated earlier, to optimize the performance of SVR models, a grid search was applied on the normalized data and the best combination of the hyper-parameters is identified for each kernel type. Table 10 presents the final optimal combination for each SVR model's kernel type along with the corresponding the best ( $R^2$ ) and ( $RMSE$ ) obtained during finer grid search. For instance, in RBF SVR model, 4725 number of combinations of hyper-parameters is considered during coarse grid search, and region with the optimal solution was identified. Fig. 11, presents the evolution of the hyper-parameters ( $C$ ), ( $\epsilon$ ) and ( $\gamma$ ) in function of ( $R^2$ ) and ( $RMSE$ ), while the remaining two hyper-parameters are at their optimal values. The best combination corresponds to the pairs ( $C, \epsilon, \gamma$ ) that have simultaneously the highest possible ( $R^2$ ) and the lowest ( $RMSE$ ). For example, as observed in Fig. 11a and b, ( $C$ ) reaches its minimal ( $RMSE$ ) and higher ( $R^2$ ) in the interval between  $2^1$  and  $2^3$ . Hence, a finer grid search was conducted in this interval with a step size of  $0.25$  in the power scale to find the final optimal solution. Similarly, for ( $\gamma$ ), a finer grid search was performed in the interval of  $2^{-1}$  and  $2^1$  with a step size of  $0.25$  in the power scale.

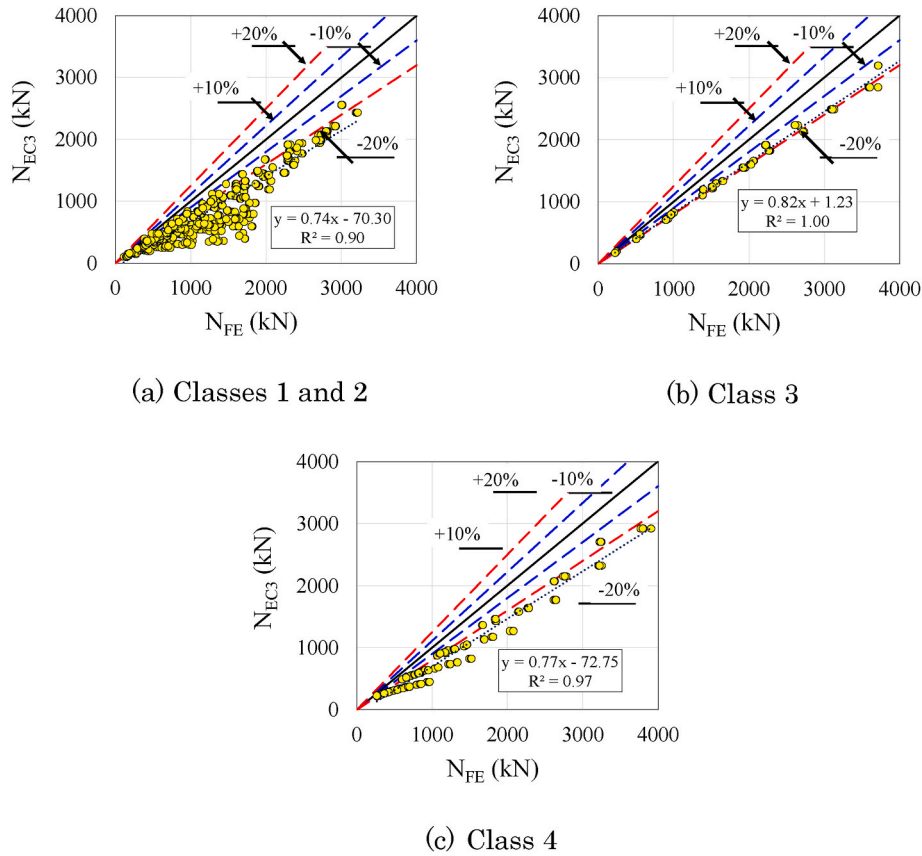


Fig. 9. Comparison of results considering the class of cross-section.

**Table 8**  
Statistical analysis for the  $N_{EC3}/N_{FE}$  ratio considering the type of stainless steel.

Stainless steel	Mean	S.D (%)	CoV (%)	$R^2$
Austenitic	0.668	13.2 %	19.8 %	0.8978
Duplex	0.698	9.7 %	13.8 %	0.9735
Ferritic	0.777	10.1 %	12.9 %	0.9776

**Table 9**  
Statistical analysis for the  $N_{EC3}/N_{FE}$  ratio considering the class of cross-section.

Class	Mean	S.D (%)	CoV (%)	$R^2$
1 and 2	0.674	13.8 %	20.4 %	0.8969
3	0.817	2.6 %	3.1 %	0.9965
4	0.693	9.4 %	13.6 %	0.9719

Moreover, ( $\epsilon$ ) achieves minimal ( $RMSE$ ) and maximal ( $R^2$ ) all through the interval from  $2^{-15}$  up to  $2^{-8}$ , and both performance metrics remain constant within this range, as depicted in Fig. 11e and f. As illustrated in Fig. 12, there is a strong correlation between error tolerance ( $\epsilon$ ) and the percentage (or number) of support vectors. Specifically, increasing ( $\epsilon$ ) while ( $C$ ) and ( $\gamma$ ) are fixed at their optimal values, leads to a decrease in the number of support vectors, resulting in a less complicated SVR model. This highlights the findings of other research studies such as (Wei and He, 2023; Chen and Yu, 2007). Fig. 12 also depicts the evolution of ( $RMSE$ ) with respect to ( $\epsilon$ ) while the remaining two hyper-parameters are fixed. Accordingly, a refined grid search is conducted in interval of  $2^{-11}$  and  $2^{-8}$  with a step size of 0.25 in the power scale, and the optimal value of ( $\epsilon$ ) was selected within this range based on three criteria: minimal ( $RMSE$ ), higher ( $R^2$ ) and reduced number of SVs.

Fig. 13 shows comparisons between the predicted the cross-section

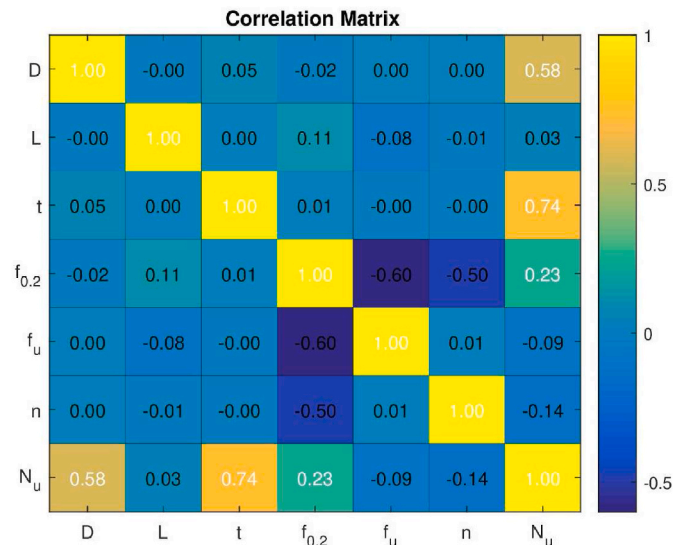
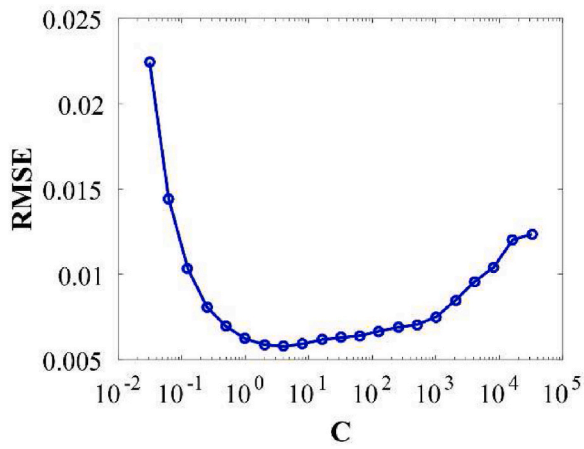


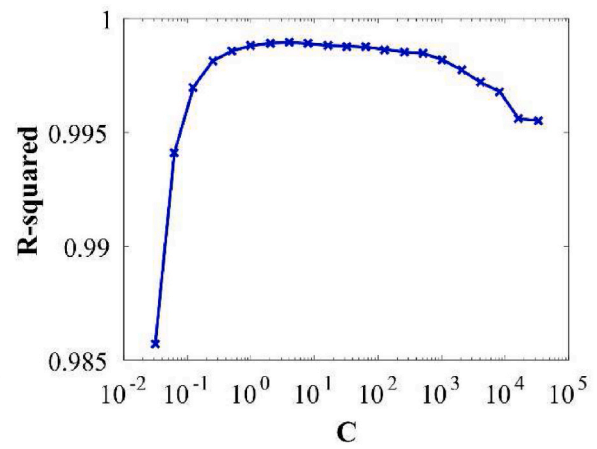
Fig. 10. Pearson's correlation matrix for the current dataset.

**Table 10**  
Optimal hyper-parameters and corresponding  $RMSE$  and  $R^2$  \*  $RSME$  corresponds to normalized data.

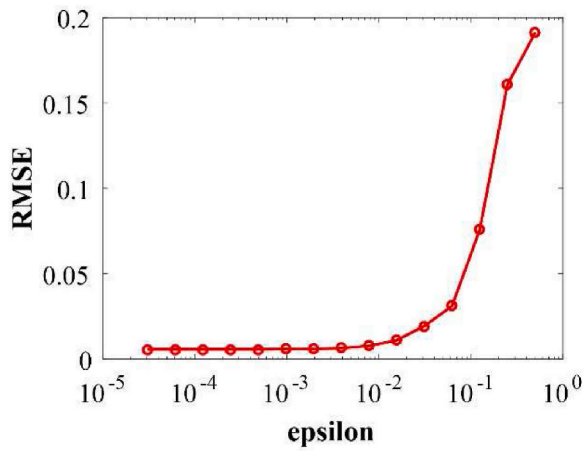
Kernel type	$C$	$\epsilon$	$\gamma$	$d$	$RMSE^*$	$R^2$
Linear	$2^{-4.75}$	$2^{-3.75}$	-	-	0.059740	0.901605
Polynomial	$2^{-5}$	$2^{-7.75}$	-	6	0.006324	0.998765
RBF	$2^2$	$2^{-8.25}$	$2^0$	-	0.006315	0.998770
Sigmoid	$2^6$	$2^{-8.75}$	$2^{-5}$	-	0.005959	0.998883



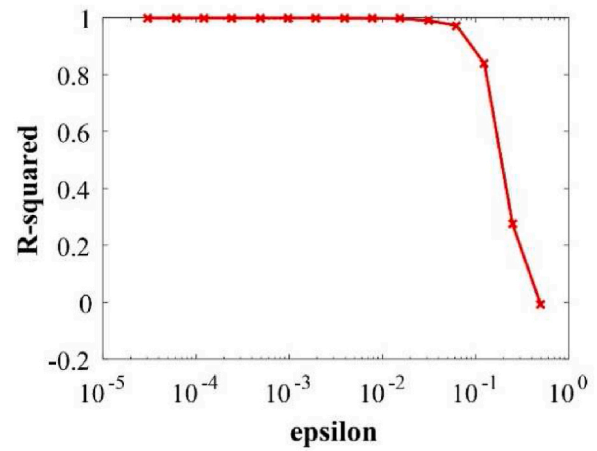
(a)



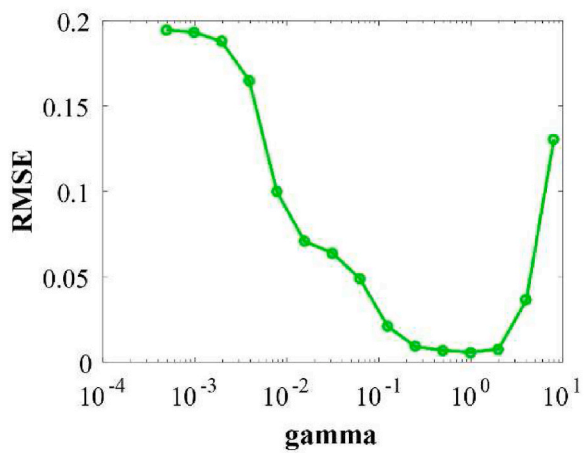
(b)



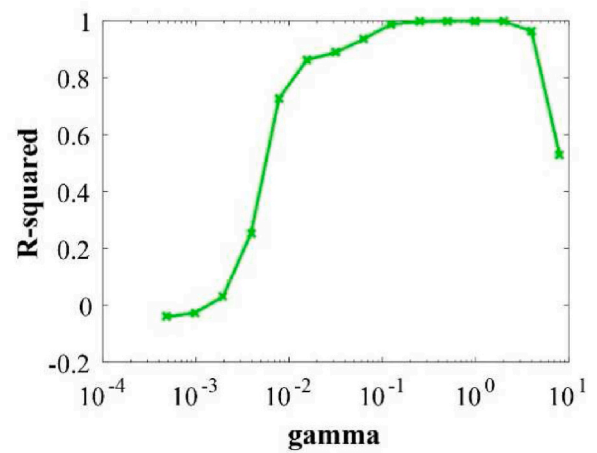
(c)



(d)



(e)



(f)

Fig. 11. Determination of optimal hyper-parameters for SVR model with RBF.

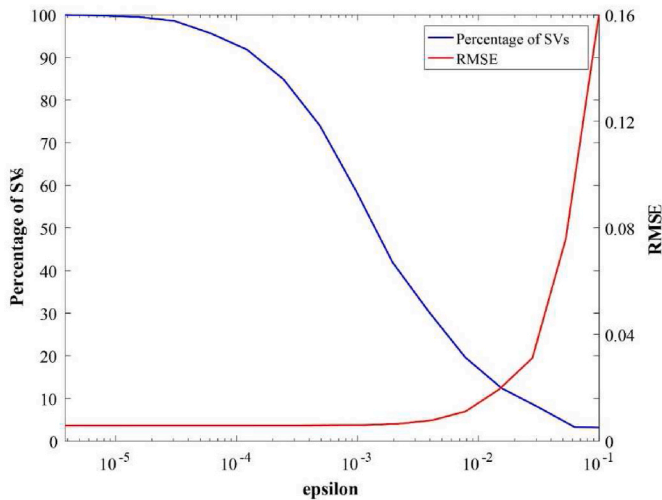


Fig. 12. Evolution of percentage of SVs and RSME as a function of  $\epsilon$ .

resistance ( $N_{SVR}$ ) using SVR with linear, polynomial, RBF, and sigmoid kernels, and those obtained from FEA ( $N_{FE}$ ), which are considered as the actual the cross-section resistance. It is clear from this figure, that there is excellent agreement between the actual and predicted results when using SVR with RBF and sigmoid kernels, followed by polynomial SVR model. Nevertheless, SVR with linear kernel falls short in accurately predicting the cross-section resistance, which is obvious due to the non-linearity of the problem. On the other hand, Polynomial SVR model provides a higher level accuracy, with an ( $R^2$ ) of 99.91 %, along with a ( $RMSE$ ) and ( $MAE$ ) of 0.0057 and 0.0035, respectively, as illustrated in Table 11. Additionally, this model achieves a percentage of support vectors of 23.73 %. Both RBF and sigmoid SVR models exhibit exceptional accuracy with an ( $R^2$ ) of 99.93 %. Furthermore, they provide the lowest ( $RMSE$ ) of approximately 0.05 and ( $MAE$ ) values of 0.0029 and 0.025, respectively. However, it is worth noting that SVR with RBF uses only 32.65 % of support vectors while with sigmoid kernel uses 35.83 %, which means the sigmoid SVR model yields a quite more complex SVR model for approximately a similar level of accuracy. Furthermore, the SVR model with sigmoid kernel uses a higher number of hyperparameters, namely ( $C, \epsilon, \gamma, r$ ), compared to the SVR model with RBF. Optimizing these hyperparameters can be time-consuming and involves higher computational resources. The same applies to the Polynomial

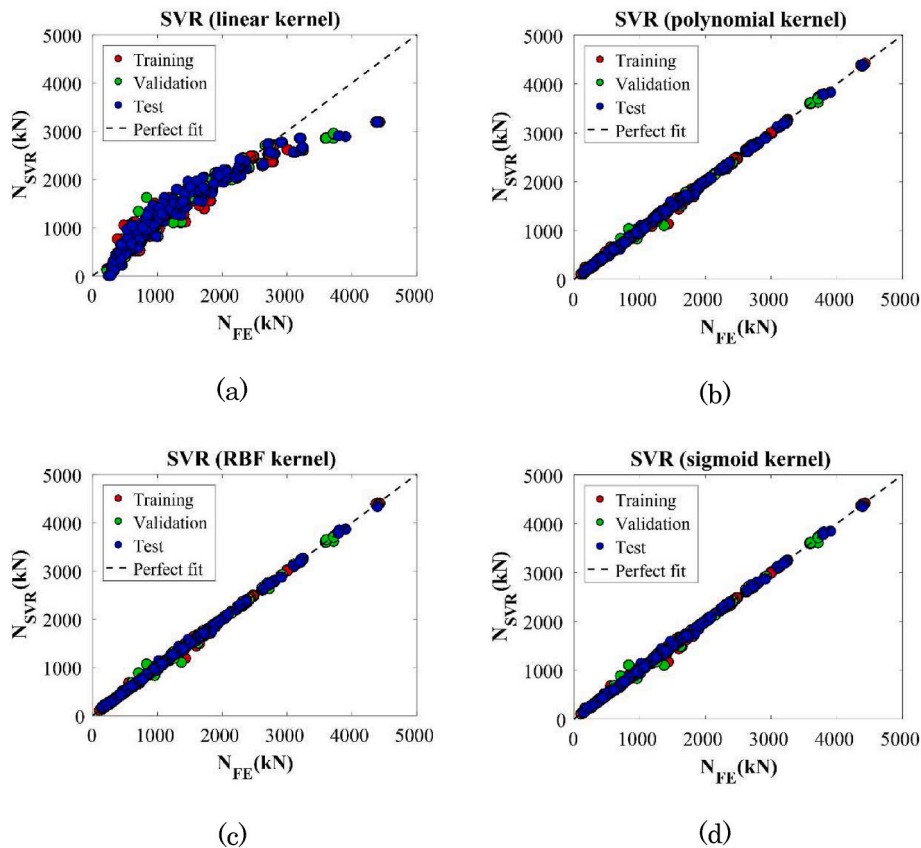


Fig. 13. Comparison between the FE and predicted results using SVR.

Table 11  
Performance metrics.

Kernel Function	Training		Validation		Testing		All data		
	$R^2$	$RMSE$	$R^2$	$RMSE$	$R^2$	$RMSE$	$R^2$	$RMSE$	$MAE$
Linear	0.9033	0.0595	0.8982	0.0609	0.8970	0.0628	0.9035	0.0602	0.0451
Polynomial	0.9993	0.0052	0.9983	0.0078	0.9993	0.0054	0.9991	0.0057	0.0035
RBF	0.9995	0.0043	0.9981	0.0083	0.9993	0.0053	0.9993	0.0052	0.0029
Sigmoid	0.9995	0.0042	0.9981	0.0082	0.9993	0.0051	0.9993	0.0051	0.0025

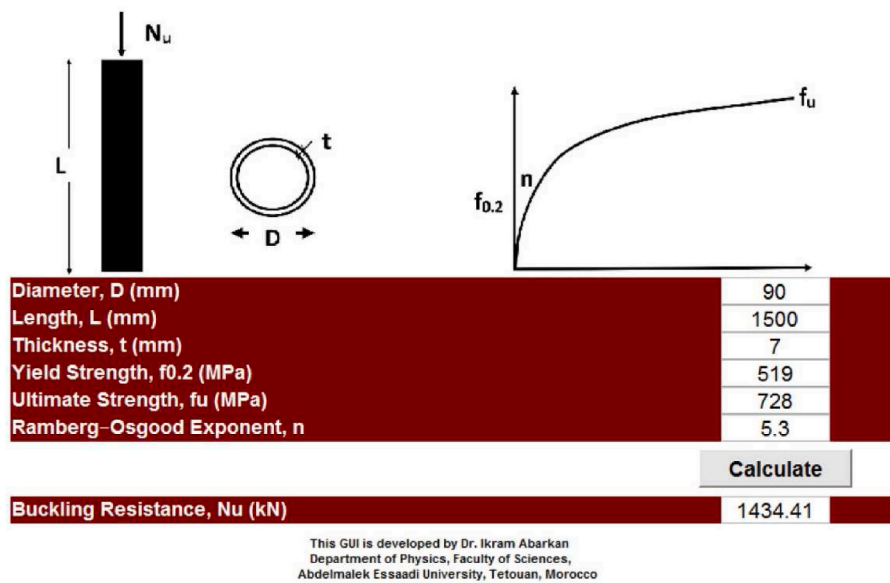


Fig. 14. Graphical user interface for SVR.

Table 12

Regression values for training, validation and testing data sets.

No. of Neurons	$R^2$			All data		
	Training	Validation	Testing	$R^2$	MAE	RMSE
4	0.9981	0.9983	0.9975	0.9961	37.3	51.6
6	0.9989	0.9984	0.9987	0.9971	27.2	40.2
8	0.9994	0.9983	0.9992	0.9985	19.0	31.6
10	0.9995	0.9992	0.9993	0.9989	15.8	27.9

SVR model, which requires also the optimization of several hyper-parameters ( $C, \epsilon, d, r$ ). Hence, based on the present investigation, the SVR model with the RBF kernel is recommended to be used in order to accurately predict the cross-section resistance of CHS stainless steel stub columns. Accordingly, this model has been implemented in the Graphical User Interface (GUI) called the cross-section resistance Calculator' using Matlab (MATLAB and Statistics Toolbox Release, 2019). As shown in Fig. 14, the user is prompted to enter the required input parameters within the range specified in Table 6 to ensure the accuracy of the results. Afterwards, the user can press the 'calculate' button to obtain the corresponding the cross-section resistance. All the installation resources to install the GUI can be found at: <https://github.com/IkramAB>

### ARKAN/SVR

#### 5.3. Prediction-based Artificial Neural Networks

Table 12 provides the regression values for the training, validation, and testing data sets. Overall, the results show a very accurate model for predicting the ultimate resistance of CHS sections. The table provides the ( $R^2$ ), ( $MAE$ ) and ( $RMSE$ ) of results when predicted results are compared to actual results. The trends that are noted in Tables 12, in which as the number of neurons in the model increase, there is an increase in the accuracy of the output. The increase in neurons also leads to more complicated formulas and potentially produces a model that is overtraining. However, using 8 neurons provides great accuracy with ( $R^2$ ), ( $MAE$ ) and ( $RMSE$ ) were 0.9985, 19.0, and 31.6, respectively. This model was converged at 180 epochs corresponding.

Fig. 15 provides the impact of input parameters using the Connection Weight Approach. For all models analysed, results show that as the values of ( $D$ ), ( $t$ ), ( $f_{0.2}$ ) and ( $f_u$ ) increase, there is an increase in the cross-section resistance and as n increases, there is a decrease in the cross-section resistance. This is physically expected as the cross-section resistance of the stainless steel CHS stub column by increasing the diameter, thickness, yield and ultimate stresses of the stainless steel.

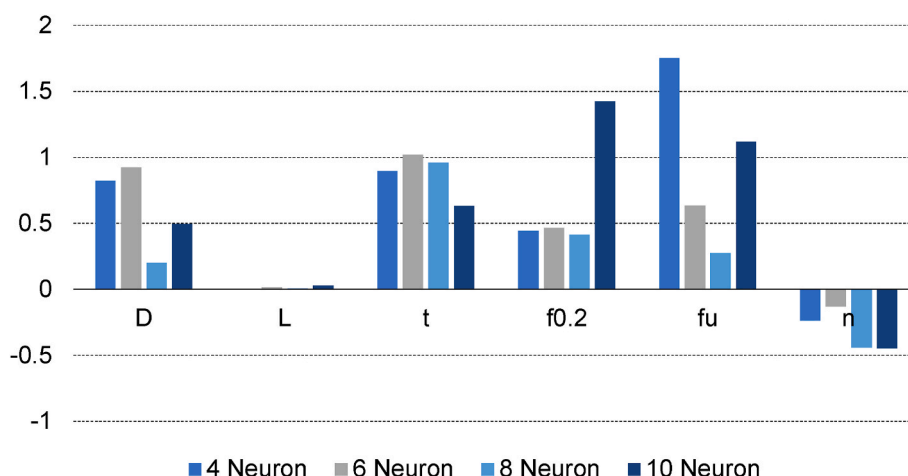


Fig. 15. Impact of input parameters- Connection Weight Approach.

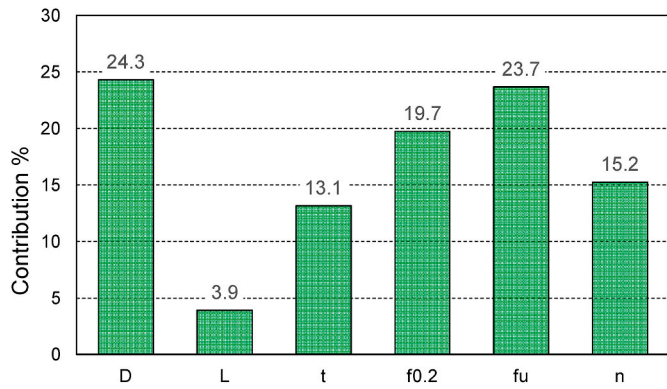


Fig. 16. Contribution (%) of input parameters to the resistance (8 neurons).

Furthermore, the diameter, thickness, and yield stress were shown to have the largest impact on cross-section resistance, while the length has insignificant impact on the capacity.

Fig. 16 illustrates the importance of the input parameters. The most important input corresponds to highest contribution value calculated using Garson algorithm as explained in section 4.2.3. It can be observed that the column diameter, yield stress and ultimate stress of the stainless steel are the significant parameters on the cross-section resistance, while the length has less effect on the resistance. The contribution of the input parameters ( $D$ ), ( $L$ ),  $t$ , ( $f_{0.2}$ ), ( $f_u$ ) and ( $n$ ) is 24.3 %, 3.9 %, 13.1 %, 19.7 %, 23.7 %, and 15.2 %, respectively. In conclusion, as the ANN model with eight neurons provides predictions with high level of accuracy and the impact of the inputs on the resistance is as physically expected, it will be used in the following sections.

The ANN model and its parameters has been implemented in user-friendly excel sheet. The user is prompted to enter the required input parameters within the range specified in Table 6 to ensure the accuracy of the results. The sheet can be found at: <https://github.com/Rabee-Shamass/ANN-for-Stainless-Steel-sub-column>.

#### 5.4. Prediction-based Gene Expression Programming

Table 13 shows the performance results of the tried GEP model. Seven models were developed to achieve the most accurate and best-fitted model for predicting the ( $N_u$ ) of the CHS stainless steel stub columns. Statistical measurements were also calculated to assess the performance of each model. A model with the highest ( $R^2$ ) and lowest errors of ( $RMSE$ ) and ( $MAE$ ) values of both datasets was considered the optimal GEP model in this study. It can be seen that the GEP 6 is the best model among all trialed GEP models. It has been generated using ( $N_c$ ) of 60, ( $H_s$ ) of 8, and ( $N_g$ ) of 4.

The regression plot of the optimal (GEP6) model utilizing the combined datasets is shown in Fig. 17. The model results with ( $R^2$ ) of 96.6 %, ( $RMSE$ ) of 152.8, and ( $MAE$ ) of 109.5. Further, the proposed model results in an average ratio of (1.08) for the “measured-to-predicted” ( $N_u$ )

values and with a 64.8 coefficient of variation. A stable level of convergence was reached at 395 iterations. The consistency of the statistical results among the training, validation, and combined datasets as well as the unity of the average ratio prove the accuracy of this model for predicting the ( $N_u$ ) values of the CHS stainless steel stub columns.

Fig. 18 shows the generated expression tree from the proposed GEP model. It consists of four genes (Sub-ET1 to Sub-ET4) that are linked together by the addition function. The symbols  $d0, d1, d2, d3, d4$ , and  $d5$  represent the input variables ( $D$ ), ( $L$ ), ( $t$ ), ( $f_{0.2}$ ), ( $f_u$ ), and ( $n$ ), respectively. The tree is also composed of constant values including:  $C5 = 8.6254$  in the first gene (Sub-ET1),  $C4 = 8.5698$  in the second gene (Sub-ET2), and  $C0 = -2.2036$  in the fourth gene (Sub-ET4). The tree is simplified mathematically in Eq. (23), which can be used to predict the  $N_u$  (kN) of the CHS stainless steel stub columns.

$$N_u = \left( \tan((-f_u) \times 8.6254 \times \ln(D))^2 \right) + \left( \frac{1.0}{n \times [(t - (n + 8.5698))^3]} \right) + \left( \sqrt[3]{\frac{D^3 - (f_u \times L)}{(f_{0.2} - f_u)^2}} \right) + \left( (t \times D) + \left( \frac{D}{-2.2036} \right) + t^3 + f_{0.2} \right) \quad (23)$$

#### 5.5. Prediction-based Decision Tree for regression

In this paper, the Decision Tree for Regression used had no limitations on the number of levels or the number of leaves. Consequently, the tree will have the same number of leaves as the length of the training dataset. Table 14 demonstrates the influence of the length of the training dataset in the overall performance of the DTR, under this architecture.

Fig. 19 shows a comparison between the predicted values of ultimate capacity ( $N_u$ ) using DTR and the values obtained from FEA. As it is evident from this Figure, the DTR algorithm is successful at predicting the FE results with an ( $R^2$ ) of 99.88 % and ( $MAE$ ) and ( $RMSE$ ) of 11.82 and 29.07, respectively. Based on this study, the tree arising from a 50-

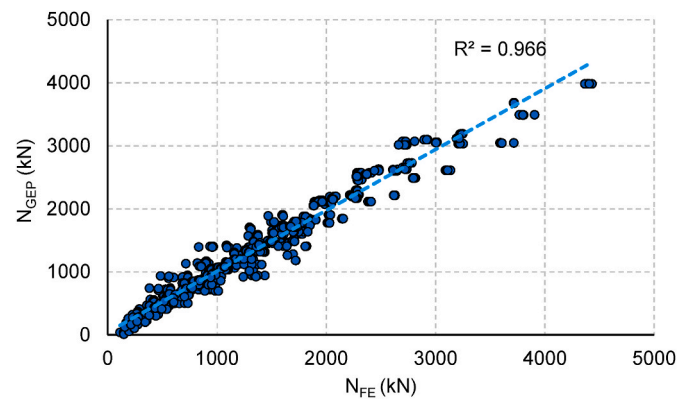


Fig. 17. Comparison between the FE and predicted results using GEP.

Table 13

Performance measures of the GEP models.

Trials	Setting Parameters			Statistical Measures						Used variables (*)
	Nc	Hs	Ng	Training dataset (70 %)			Validation dataset (30 %)			
				RMSE	MAE	R <sup>2</sup>	RMSE	MAE	R <sup>2</sup>	
GEP1	30	8	3	182.91	136.41	0.949	195.69	144.56	0.948	4
GEP2	60	8	3	183.60	136.08	0.953	175.62	132.25	0.954	6
GEP3	90	8	3	188.57	136.25	0.951	178.08	128.03	0.953	6
GEP4	60	9	3	183.81	129.68	0.953	177.19	123.18	0.954	5
GEP5	60	10	3	187.94	143.46	0.949	196.45	150.67	0.943	5
<b>GEP6</b>	<b>60</b>	<b>8</b>	<b>4</b>	<b>149.31</b>	<b>107.15</b>	<b>0.967</b>	<b>160.79</b>	<b>115.05</b>	<b>0.963</b>	<b>6</b>
GEP7	60	8	5	180.55	132.97	0.953	174.42	129.70	0.955	6

Note: The bold row indicates the ideal GEP model; (\*) An ideal model should consider the six input variables.

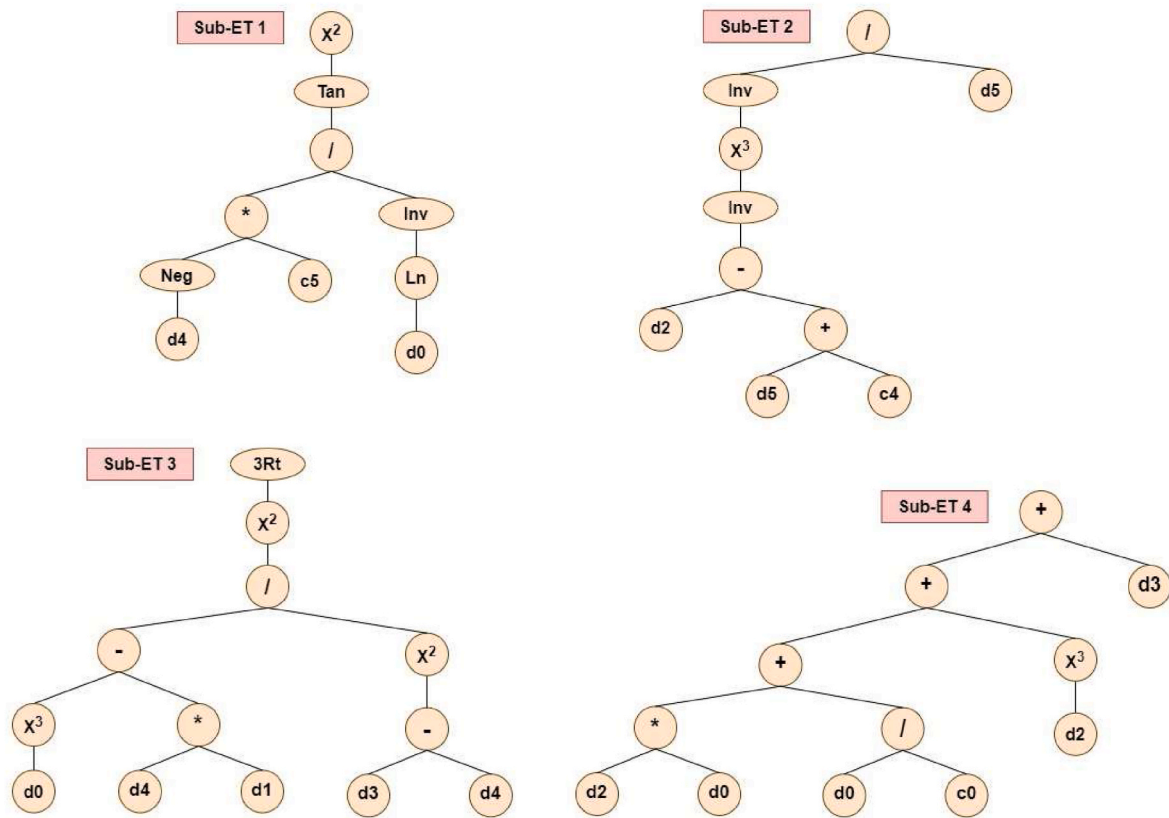


Fig. 18. Gene Expression Programming tree.

Table 14

Influence of train-test split on the accuracy of the regression trees.

Split	10-90	20-80	30-70	40-60	50-50	60-40	70-30	80-20	90-10
Training size	1371	1219	1066	914	762	609	457	304	152
Test size	153	305	458	610	762	915	1067	1220	1372
No. levels	16	15	15	16	16	14	13	12	12
No. leaves	1371	1219	1066	914	762	609	457	304	152
R <sup>2</sup>	0.9979	0.9984	0.9990	0.9983	0.9988	0.9889	0.9829	0.9618	0.9123

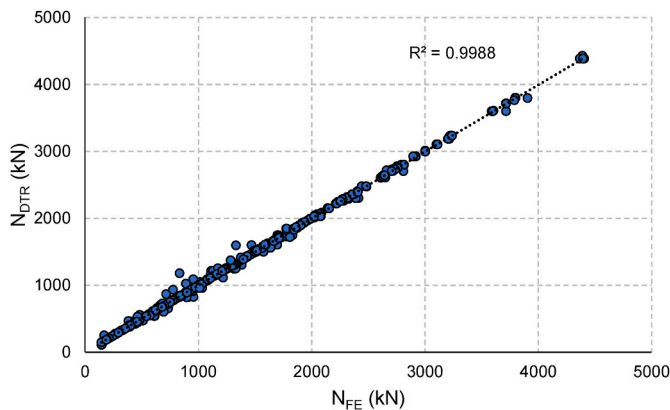
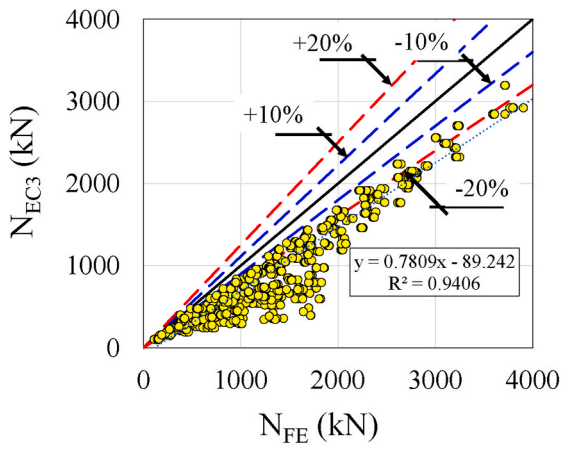


Fig. 19. Comparison between the FE and predicted results using DTR.

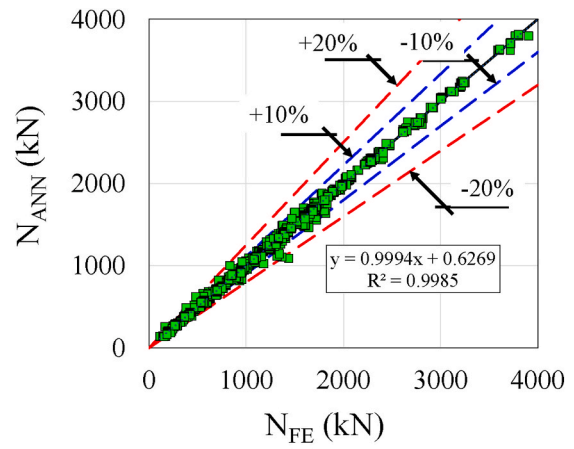
50 split of training data and test data has been considered for the comparisons with EC3 and other machine learning algorithms. The Python code for the DTR can be found here:

### 6. Comparison between Eurocode 3, ANN, SVR, GEP and DTR predictions

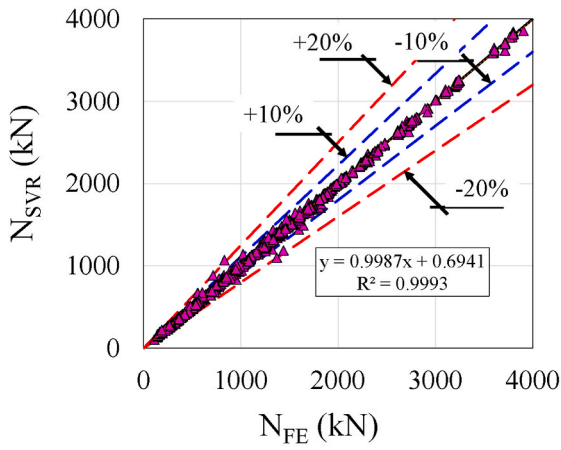
In this section, the predicted models presented previously are compared with finite element models (Fig. 20). Considering the EC3 predictions in comparison with the finite element models (Fig. 20a), it was verified that the calculation model of EC3 underestimates the resistance of the CHS, with the minimum and maximum values of the relative error reaching -77 % and 5 %, respectively. Figs. 20b and c show the results of machine learning models, considering the ANN and SVR, respectively. According to the illustrations, both machine learning models accurately predict the resistance of CHS. The maximum relative error found for ANN and SVR was 54.7 % and 28.6 %, respectively, while the minimum relative error was -24.2 % and -19.8 %, considering ANN and SVR, respectively. Fig. 20d shows the comparisons between GEP and finite element models. The minimum and maximum relative errors were -91,1 % and 94,4 %, respectively, thus showing that the results predicted by GEP underestimate and overestimate CHS resistance. In relation to DTR model predictions (Fig. 20e), better predictions



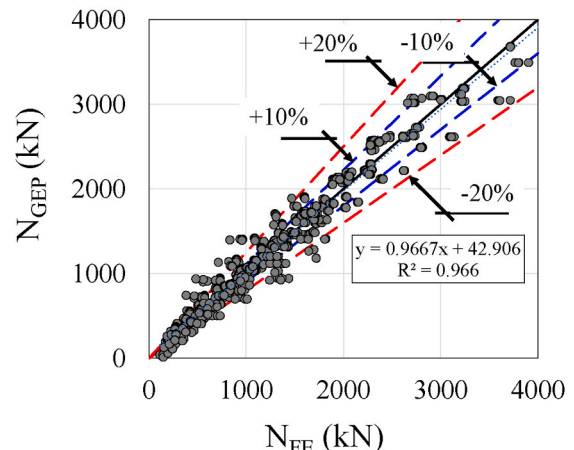
(a) EC3



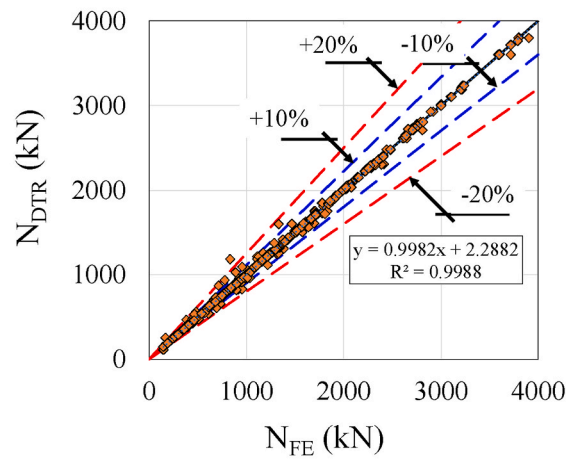
(b) ANN



(c) SVR



(d) GEP



(e) DTR

Fig. 20. Comparison between EC3, ANN, SVR, GEP and DTR predictions with finite element models.

**Table 15**  
Statistical analysis for the predicted and finite element model ratio ( $N_{Predicted}/N_{FE}$ ).

Model	EC3	ANN	SVR	GEP	DTR
Mean	0.698	1.000	1.000	0.996	1.000
S.D	12.65 %	3.88 %	2.73 %	18.39 %	3.76 %
$R^2$	0.9406	0.9985	0.9993	0.966	0.9988
MAE	363.15	19.0	12.7	109.52	11.82
RMSE	437.3	31.6	22.6	152.84	29.07
Minimum error ( $N_{Predicted}/N_{FE}-1$ )	-76.9 %	-24.2 %	-19.8 %	-92.1 %	-24.5 %
Maximum error ( $N_{Predicted}/N_{FE}-1$ )	4.5 %	54.7 %	28.6 %	94.4 %	49.7 %

**Table 16**  
Summary of the reliability analysis calculated according to EN 1990 (European committee for standardization).

Model	$n$	$\bar{b}$	$k_{d,n}$	$k_n$	$V_r$	$\gamma_{M0}$
EC3	1524	1.335	3.04	1.65	0.235	1.38
ANN	1524	0.999	3.04	1.65	0.101	1.15
SVR	1524	1.000	3.04	1.65	0.097	1.15
GEP	1524	1.000	3.04	1.65	0.272	1.45
DTR	762	1.000	3.04	1.65	0.100	1.15

were identified compared to the GEP model, since the minimum and maximum relative errors were equal to -24.5 % and 49.8 %, respectively. Table 15 presents the statistical results of the five prediction models. It can be noted that both machine learning algorithms provided better predictions than EC3 since the (RMSE) and (MAE) values for the EC3 predictions were much higher than those for the ANN, SVR, GEP and DTR predictions.

## 7. Reliability analysis based on annex D EN 1990

In this section, reliability analysis based on Annex D EN 1990 (2002) (European committee for standardization) has been conducted to assess the reliability of the machine learning method and EC3 prediction and propose a partial safety factor for the cross-section resistance of a circular hollow section (CHS) stainless steel stub column. In the framework of the present study the statistical evaluation of the proposed prediction models is done here against the finite element results. Table 16 illustrates the key statistical parameters, including the number of data,  $n$ , the design fractile factor (ultimate limit state),  $k_{d,n}$ , the characteristic fractile factor,  $k_n$  the average ratio of FE to resistance model predictions based on the least squares fit to the data,  $\bar{b}$ , the combined coefficient of variation incorporating both resistance model and basic variable uncertainties,  $V_r$ , and the partial safety factor for resistance  $\gamma_{M0}$ . The COV of geometric dimensions of steel is 0.05 (Afshan et al., 2015). The COV of the yield strength of stainless steel, and ultimate strength of the stainless steel were assumed equal to 0.06 (Afshan et al., 2015) and 0.035 (Afshan et al., 2015), respectively. The COV between the experimental and the numerical results, which was found equal to 0.0381, was also considered. Performing First Order Reliability Method (FORM) in accordance with the Eurocode target reliability requirements, the partial factors  $\gamma_{M0}$  were evaluated for all ML models and EC3 prediction. As can be seen from Table 16, the partial factor for the cross-section capacity based on the GEP algorithm is the highest among the other ML models while it is 1.15 based on the ANN, SVR and DTR. The partial factor based on the EC3 is 1.38. It can be concluded that ANN, SVR and DTR provided the better prediction than that EC3 and GEP.

## 8. Concluding remarks

This paper studied the cross-section resistance of stainless steel CHS

stub columns subjected to axial loadings. Firstly, numerical modeling was conducted to validate the FE models. Based on this validation, a parametric study was carried out to extend the data range, resulting in a dataset of 1524 samples with various geometrical dimensions, material grades, and properties. This data was used to train, validate, and test the ANN, GEP, DTR models, and SVR models with four kernels: linear, polynomial, RBF, and sigmoid. Although stainless steel material has many advantages when used in structural members, the initial cost is very high. Therefore, machine learning models have been utilized to suggest design that optimizes material usage and improves efficiency. The predicted results using ANN, SVR, GEP and DTR were compared with FE and EC3 to assess their accuracy. Accordingly, the following conclusions are made:

- The EC3 provides very conservative predictions of the numerical counterparts with the mean and CoV values of the  $N_{EC3}/N_{FE}$  ratio were around 0.67 and 19.8 % for austenitic stainless steel, 0.70 and 13.8 % for duplex stainless steel and 0.78 and 12.9 % for ferritic stainless steel. This is mainly owing to neglecting the blatant difference in the material stress-strain behavior of stainless steel compared with that of carbon steel.
- Among the SVR models, those with RBF and sigmoid kernels achieved the highest level of accuracy, with an ( $R^2$ ) value of 0.9993 and (RMSE) of 0.005. The polynomial kernel also performed well, with an ( $R^2$ ) value of 0.9991 and an (RMSE) of 0.0057. However, the linear kernel failed to accurately predict the cross-section resistance. The SVR model with RBF was found to provide the most accurate results with less computational complexity compared to other kernels.
- The ANN model accurately predicts the cross-section resistance of the stainless steel stub columns with an  $R^2$  value of 0.9985 and RMSE and MAE values equal 31.6 and 19.0, respectively. However, SVR with RBF performed better than ANN, GEP, and DTR with ( $R^2$ ), (RMSE) and (MAE) values of 0.9993, 22.6 and 12.7, respectively. GEP provided the lowest level of accuracy than that for the other three machine learning methods.
- The machine learning algorithms investigated in this study performed much better than the EC3 design, in which ( $R^2$ ), (RMSE) and (MAE) values for the latter are 0.9406, 437.3 and 363.15, respectively. Therefore, SVR was implemented in the GUI, and ANN was implemented in user-friendly excel sheet enabling engineering practitioner to predict easily the cross-section resistance of CHS stainless steel stub columns. A straightforward equation (i.e. Eq. (23)) generated from GEP method can also be used to predict the capacity. It should be noted that the load capacity calculated should be divided by the partial factors proposed in Table 16.
- Further research study is application of machine learning to predict the capacity of other stainless steel members such as columns under eccentric loading. Another interesting study is to use the ML to classify the failure mode of structural stainless steel members.

## CRedit authorship contribution statement

**Ikram Abarkan:** Writing – original draft, Visualization, Validation, Software, Methodology, Investigation, Conceptualization. **Musab Rabi:** Writing – original draft, Validation, Methodology, Investigation, Conceptualization. **Felipe Piana Vendramell Ferreira:** Writing – original draft, Validation, Software, Methodology, Investigation, Conceptualization. **Rabee Shamass:** Writing – original draft, Software, Methodology, Investigation, Formal analysis. **Vireen Limbachiya:** Writing – original draft, Software, Methodology, Investigation, Conceptualization. **Yazeed S. Jweihan:** Writing – original draft, Software, Methodology, Investigation. **Luis Fernando Pinho Santos:**

Writing – original draft, Validation, Software, Methodology, Investigation, Conceptualization.

### Declaration of competing interest

The authors declare that they have no known competing financial interests or personal relationships that could have appeared to influence the work reported in this paper.

### Data availability

Data will be made available on request.

### References

- Abellán-García, J., 2020. Four-layer perceptron approach for strength prediction of UHPC. *Construct. Build. Mater.* 256, 119465.
- Afshan, S., Gardner, L., 2013a. Experimental study of cold-formed ferritic stainless steel hollow sections. *J. Struct. Eng.* 139 (5), 717–728.
- Afshan, S., Gardner, L., 2013b. The continuous strength method for structural stainless steel design. *Thin-Walled Struct.* 68, 42–49.
- Afshan, S., Francis, P., Baddoo, N.R., Gardner, L., 2015. Reliability analysis of structural stainless steel design provisions. *J. Constr. Steel Res.* 114, 293–304. <https://doi.org/10.1016/j.jcsr.2015.08.012>.
- Almomani, Y., Tarawneh, A., Alawadi, R., Taqieddin, Z.N., Jweihan, Y.S., Saleh, E., 2023. Predictive models of behavior and capacity of frp reinforced concrete columns. *Journal of Applied Engineering Science* 21 (1), 143–156.
- Anosri, S., Panagant, N., Champasak, P., Bureerat, S., Thipyopas, C., Kumar, S., et al., 2023. A comparative study of state-of-the-art metaheuristics for solving many-objective optimization problems of fixed wing unmanned aerial vehicle conceptual design. *Arch. Comput. Methods Eng.* 1–15.
- Apicella, A., Donnarumma, F., Isgrò, F., Prevete, R., 2021. A survey on modern trainable activation functions. *Neural Network.* 138, 14–32.
- AS/NZS 4673, 2001. Cold-formed Stainless Steel Structures, 4673. AS/NZS, Sydney, p. 2001.
- Ashraf, M., Gardner, L., Nethercot, D.A., 2008. Structural stainless steel design: resistance based on deformation capacity. *J. Struct. Eng.* 134 (3), 402–411.
- Ashraf, Waqar Muhammad, et al., 2021. Strategic-level performance enhancement of a 660 MWe supercritical power plant and emissions reduction by AI approach. *Energy Convers. Manag.* 250, 114913.
- Awad, M., Khanna, R., Awad, M., Khanna, R., 2015. Support vector regression. Efficient learning machines: Theories, concepts, and applications for engineers and system designers 67–80.
- Aye, C.M., Pholdee, N., Yildiz, A.R., Bureerat, S., Sait, S.M., 2019. Multi-surrogate-assisted metaheuristics for crashworthiness optimisation. *Int. J. Veh. Des.* 80 (2–4), 223–240.
- Bardi, F.C., Kyriakides, S., 2006. Plastic buckling of circular tubes under axial compression—part I: experiments. *Int. J. Mech. Sci.* 48 (8), 830–841.
- Becque, J., Rasmussen, K.J., 2009. Experimental investigation of local-overall interaction buckling of stainless steel lipped channel columns. *J. Constr. Steel Res.* 65 (8–9), 1677–1684.
- Breiman, L., 2017. *Classification and Regression Trees*. Routledge.
- Buchanan, C., Gardner, L., Liew, A., 2016. The continuous strength method for the design of circular hollow sections. *J. Constr. Steel Res.* 118, 207–216.
- Buchanan, C., Real, E., Gardner, L., 2018. Testing, simulation and design of cold-formed stainless steel CHS columns. *Thin-Walled Struct.* 130, 297–312.
- Chen, S.T., Yu, P.S., 2007. Pruning of support vector networks on flood forecasting. *J. Hydrol.* 347 (1–2), 67–78. <https://doi.org/10.1016/j.jhydrol.2007.08.029>.
- Cortes, C., Vapnik, V., 1995. Support-vector networks. *Mach. Learn.* 20 (3), 273–297.
- Dai, Y., Roy, K., Fang, Z., Chen, B., Raftery, G.M., Lim, J.B., 2022a. A novel machine learning model to predict the moment capacity of cold-formed steel channel beams with edge-stiffened and un-stiffened web holes. *J. Build. Eng.* 53, 104592.
- Dai, Y., Roy, K., Fang, Z., Raftery, G.M., Jim, J.B., 2022b. Moment capacity of cold-formed steel channel beams with edge-stiffened holes by machine learning. *Cold-Formed Steel Research Consortium. CFSRC Colloquium*.
- Dassault Systèmes Simulia, 2016. *Abaqus 6.18*.
- Dissanayake, M., Nguyen, H., Poologanathan, K., Perampalam, G., Upasiri, I., Rajanayagam, H., Suntharalingam, T., 2022. Prediction of shear capacity of steel channel sections using machine learning algorithms. *Thin-Walled Struct.* 175, 109152.
- Du, Y., Chen, Z., Zhang, C., Cao, X., 2017. Research on axial bearing capacity of rectangular concrete-filled steel tubular columns based on artificial neural networks. *Front. Comput. Sci.* 11, 863–873.
- D'Aniello, M., Güneş, E.M., Landolfo, R., Mermerdaş, K., 2015. Predictive models of the flexural overstrength factor for steel thin-walled circular hollow section beams. *Thin-Walled Struct.* 94, 67–78.
- EN 1993-1-4, Eurocode 3: Design of Steel Structures – Part 1.4: General Rules – Supplementary Rules for Stainless Steels, 2006. European Committee for Standardization (CEN), Brussels.
- European Committee for Standardization, EN 1990: Eurocode – Basis of Structural Design, (n.d.).
- European Committee for Standardization, 2020. prEN 1993-1-1: Eurocode 3 - Design of Steel Structures - Part 1-1: General Rules and Rules for Buildings. Final document, Brussels.
- Fang, Z., Roy, K., Chen, B., Sham, C.W., Hajirasouliha, I., Lim, J.B., 2021a. Deep learning-based procedure for structural design of cold-formed steel channel sections with edge-stiffened and un-stiffened holes under axial compression. *Thin-Walled Struct.* 166, 108076.
- Fang, Z., Roy, K., Mares, J., Sham, C.W., Chen, B., Lim, J.B., 2021b. Deep learning-based axial capacity prediction for cold-formed steel channel sections using Deep Belief Network. In: *Structures*, 33. Elsevier, pp. 2792–2802.
- Fang, Z., Roy, K., Dai, Y., Lim, J.B., 2022. Structural behavior of cold-formed steel channel sections with edge-stiffened and un-stiffened holes under axial compression: numerical simulations, deep learning, and proposed design equations. *Cold-Formed Steel Research Consortium (CFSRC) Colloquium*.
- Ferreira, C., 2001. Gene Expression Programming: a New Adaptive Algorithm for Solving Problems. *arXiv Preprint Cs/0102027*.
- Ferreira, C., 2002. Gene Expression Programming in Problem Solving. *Soft Computing and Industry: Recent Applications*, pp. 635–653.
- Ferreira, F.P.V., Shamass, R., Limbachiya, V., Tsavdaridis, K.D., Martins, C.H., 2022. Lateral-torsional buckling resistance prediction model for steel cellular beams generated by Artificial Neural Networks (ANN). *Thin-Walled Struct.* 170, 108592.
- Fletcher, T., 2009. Support Vector Machines Explained. Tutorial paper, pp. 1–19.
- Friedman, J.H., 2001. Greedy function approximation: a gradient boosting machine. *Ann. Stat.* 1189–1232.
- Friedman, J.H., 2002. Stochastic gradient boosting. *Comput. Stat. Data Anal.* 38 (4), 367–378.
- Garson, D.G., 1991. Interpreting Neural Network Connection Weights. *Gene, GeneXproTools*, 2000. Expression Programming Tools. Gepsoft Limited, p. 73.
- Gholizadeh, S., Pirmoz, A., Attarnejad, R., 2011. Assessment of load carrying capacity of castellated steel beams by neural networks. *J. Constr. Steel Res.* 67 (5), 770–779.
- Golafshani, E.M., Rahai, A., Sebt, M.H., Akbarpour, H., 2012. Prediction of bond strength of spliced steel bars in concrete using artificial neural network and fuzzy logic. *Construct. Build. Mater.* 36, 411–418.
- Graciano, C., Kurtoglu, A.E., Casanova, E., 2021. Machine learning approach for predicting the patch load resistance of slender austenitic stainless steel girders. In: *Structures*, 30. Elsevier, pp. 198–205.
- Güneyisi, E.M., D'Aniello, M., Landolfo, R., Mermerdaş, K., 2014. Prediction of the flexural overstrength factor for steel beams using artificial neural network. *Steel Compos. Struct.* 17 (3), 215–236.
- Gupta, T., Patel, K.A., Siddique, S., Sharma, R.K., Chaudhary, S., 2019. Prediction of mechanical properties of rubberised concrete exposed to elevated temperature using ANN. *Measurement* 147, 106870.
- Hosseinpour, M., Sharifi, Y., Sharifi, H., 2020. Neural network application for distortional buckling capacity assessment of castellated steel beams. In: *Structures*, 27. Elsevier, pp. 1174–1183.
- Hsu, C.W., Chang, C.C., Lin, C.J., 2003. *A Practical Guide to Support Vector Classification*.
- Huang, Y., Young, B., 2013. Experimental and numerical investigation of cold-formed lean duplex stainless steel flexural members. *Thin-Walled Struct.* 73, 216–228.
- Huang, M.W., Chen, C.W., Lin, W.C., Ke, S.W., Tsai, C.F., 2017. SVM and SVM ensembles in breast cancer prediction. *PLoS One* 12 (1), e0161501.
- Iqbal, J., Saeed, A., Khan, R.A., 2023. The relative importance of textual indexes in predicting the future performance of banks: a connection weight approach. *Borsa Istanbul Review* 23 (1), 240–253.
- Jweihan, Y.S., 2023. Predictive model of asphalt mixes' theoretical maximum specific gravity using gene expression programming. *Results in Engineering*, 101242.
- Jweihan, Y.S., Al-Kheetan, M.J., Rabi, M., 2023. Empirical model for the retained stability index of asphalt mixtures using hybrid machine learning approach. *Applied System Innovation* 6 (5), 93.
- Karatzoglou, A., Meyer, D., Hornik, K., 2006. Support vector machines in R. *J. Stat. Software* 15, 1–28. <https://doi.org/10.18637/jss.v015.i09>.
- Kari, T., Gao, W., Tuluhong, A., Yaermaimaiti, Y., Zhang, Z., 2018a. Mixed kernel function support vector regression with genetic algorithm for forecasting dissolved gas content in power transformers. *Energies* 11, 2437. <https://doi.org/10.3390/en11092437>.
- Kari, T., Gao, W., Tuluhong, A., Yaermaimaiti, Y., Zhang, Z., 2018b. Mixed kernel function support vector regression with genetic algorithm for forecasting dissolved gas content in power transformers. *Energies* 11, 2437. <https://doi.org/10.3390/en11092437>.
- Khan, K., Iqbal, M., Raheel, M., Amin, M.N., Alabdullah, A.A., Abu-Arab, A.M., Jalal, F. E., 2022. Prediction of axial capacity of concrete filled steel tubes using gene expression programming. *Materials* 15 (19), 6969.
- Kiyamaz, G., 2005. Strength and stability criteria for thin-walled stainless steel circular hollow section members under bending. *Thin-Walled Struct.* 43 (10), 1534–1549.
- Kuwamura, H., 2003. Local buckling of thin-walled stainless steel members. *Steel Structures* 3 (3), 191–201.
- Lau, H.L., Wong, F.W.F., Abd Rahman, R.N.Z.R., Mohamed, M.S., Ariff, A.B., Hii, S.L., 2023. Optimization of fermentation medium components by response surface methodology (RSM) and artificial neural network hybrid with genetic algorithm (ANN-GA) for lipase production by *Burkholderia cenocepacia* ST8 using used automotive engine oil as substrate. *Biocatal. Agric. Biotechnol.* 50, 102696.
- Liew, A., Gardner, L., 2015. Ultimate capacity of structural steel cross-sections under compression, bending and combined loading. In: *Structures*, 1. Elsevier, pp. 2–11.
- Limbachiya, V., Shamass, R., 2021. Application of artificial neural networks for web-post shear resistance of cellular steel beams. *Thin-Walled Struct.* 161, 107414.

- Lin, K.M., Lin, C.J., 2003. A study on reduced support vector machines. *IEEE Trans. Neural Network.* 14 (6), 1449–1459. <https://doi.org/10.1109/TNN.2003.820828>.
- Malami, S.I., Anwar, F.H., Abdulrahman, S., Haruna, S.I., Ali, S.I.A., Abba, S.I., 2021. Implementation of hybrid neuro-fuzzy and self-turning predictive model for the prediction of concrete carbonation depth: a soft computing technique. *Results in Engineering* 10, 100228.
- MATLAB and Statistics Toolbox Release 2019a, 2019. The MathWorks, Inc., Natick, Massachusetts, United States.
- Meng, X., Gardner, L., Sadowski, A.J., Rotter, J.M., 2020. Elasto-plastic behaviour and design of semi-compact circular hollow sections. *Thin-Walled Struct.* 148, 106486 <https://doi.org/10.1016/j.tws.2019.106486>.
- Meng, Z., Qian, Q., Xu, M., Yu, B., Yıldız, A.R., Mirjalili, S., 2023a. PINN-FORM: a new physics-informed neural network for reliability analysis with partial differential equation. *Comput. Methods Appl. Mech. Eng.* 414, 116172.
- Meng, Z., Yıldız, B.S., Li, G., Zhong, C., Mirjalili, S., Yıldız, A.R., 2023b. Application of state-of-the-art multiobjective metaheuristic algorithms in reliability-based design optimization: a comparative study. *Struct. Multidiscip. Optim.* 66 (8), 191.
- Müller, A., Taras, A., 2022a. Prediction of the load-displacement and local buckling behavior of hollow structural sections using Deep Neural Networks (DNN). In: *Proceedings of the Annual Stability Conference Structural Stability*. Research Council, p. 19.
- Müller, A., Taras, A., 2022b. Prediction of the local buckling strength and load-displacement behaviour of SHS and RHS members using deep neural networks (DNN)—Introduction to the deep neural network direct stiffness method (DNN-DSM). *Steel Construction* 15 (S1), 78–90.
- Müller, A., Taras, A., Kraus, M.A., 2022. Scientific machine and deep learning investigations of the local buckling behaviour of hollow sections. *ce/papers* 5 (4), 1034–1042.
- Nguyen, Q.H., Ly, H.B., Le, T.T., Nguyen, T.A., Phan, V.H., Tran, V.Q., Pham, B.T., 2020. Parametric investigation of particle swarm optimization to improve the performance of the adaptive neuro-fuzzy inference system in determining the buckling capacity of circular opening steel beams. *Materials* 13 (10), 2210.
- Nguyen, H., Vu, T., Vo, T.P., Thai, H.T., 2021a. Efficient machine learning models for prediction of concrete strengths. *Construct. Build. Mater.* 266, 120950 <https://doi.org/10.1016/j.conbuildmat.2020.120950>.
- Nguyen, T.H., Tran, N.L., Nguyen, D.D., 2021b. Prediction of critical buckling load of web tapered I-section steel columns using artificial neural networks. *International Journal of Steel Structures* 21 (4), 1159–1181.
- Nguyen, H., Vu, T., Vo, T.P., Thai, H.T., 2021c. Efficient machine learning models for prediction of concrete strengths. *Construct. Build. Mater.* 266, 120950 <https://doi.org/10.1016/j.conbuildmat.2020.120950>.
- Nguyen, T.H., Nguyen, D.X., Nguyen, T.T.T., Phan, V.L., Nguyen, D.D., 2023. Machine learning models for predicting the axial compression capacity of cold-formed steel elliptical hollow section columns. *Asian Journal of Civil Engineering* 1–13.
- Niu, S., Rasmussen, K.J., Fan, F., 2014. Distortional–global interaction buckling of stainless steel C-beams: Part I—experimental investigation. *J. Constr. Steel Res.* 96, 127–139.
- Olden, J.D., Joy, M.K., Death, R.G., 2004. An accurate comparison of methods for quantifying variable importance in artificial neural networks using simulated data. *Ecol. Model.* 178 (3), 389–397.
- Pearson, K., 1895. Note on regression and inheritance in the case of two parents. *Proc. Roy. Soc. Lond.* 58, 240–242. <https://doi.org/10.1098/rspl.1895.0041>.
- Pedregosa, F., Varoquaux, G., Gramfort, A., Michel, V., Thirion, B., Grisel, O., et al., 2011. Scikit-learn: machine learning in Python. *J. Mach. Learn. Res.* 12, 2825–2830.
- Pu, Y., Mesbahi, E., 2006. Application of artificial neural networks to evaluation of ultimate strength of steel panels. *Eng. Struct.* 28 (8), 1190–1196.
- Rabi, M., 2023. Bond prediction of stainless-steel reinforcement using artificial neural networks. *Proceedings of the Institution of Civil Engineers-Construction Materials* 1–11.
- Rabi, M., Cashell, K.A., Shamass, R.J.E.S., 2019. Flexural Analysis and Design of Stainless Steel Reinforced Concrete Beams, 198. *Engineering Structures*, 109432.
- Rabi, M., Cashell, K.A., Shamass, R., Desnerck, P., 2020. Bond behaviour of austenitic stainless steel reinforced concrete. *Eng. Struct.* 221, 111027.
- Rabi, M., Cashell, K.A., Shamass, R., 2021. Ultimate behaviour and serviceability analysis of stainless steel reinforced concrete beams. *Eng. Struct.* 248, 113259.
- Rabi, M., Shamass, R., Cashell, K.A., 2022a. Structural performance of stainless steel reinforced concrete members: a review. *Construct. Build. Mater.* 325, 126673.
- Rabi, M., Shamass, R., Cashell, K.A., 2022b. Experimental investigation on the flexural behaviour of stainless steel reinforced concrete beams. *Structure and Infrastructure Engineering* 1–13.
- Rabi, M., Ferreira, F.P.V., Abarkan, I., Limbachiya, V., Shamass, R., 2023a. Prediction of the cross-sectional capacity of cold-formed CHS using numerical modelling and machine learning. *Results in Engineering* 17, 100902.
- Rabi, M., Abarkan, I., Shamass, R., 2023b. Buckling resistance of hot-finished CHS beam-columns using FE modelling and machine learning. *Steel Construction*. <https://doi.org/10.1002/stco.202200036>.
- Rabi, Musab, Jweihan, Yazeed S., Abarkan, Ikram, Vendramell Ferreira, Felipe Piana, Shamass, Rabea, Limbachiya, Vireen, Daniel Tsavdaridis, Konstantinos, Pinho Santos, Luis Fernando, 2024. Machine learning-driven web-post buckling resistance prediction for high-strength steel beams with elliptically-based web openings. *Results in Engineering*, 101749. <https://doi.org/10.1016/j.rineng.2024.101749>.
- Raheem, M., Iqbal, M., Khan, R., Alam, M., Azab, M., Eldin, S.M., 2023. Application of gene expression programming to predict the compressive strength of quaternary-blended concrete. *Asian Journal of Civil Engineering* 1–14.
- Rasmussen, K.J., 2003. Full-range stress–strain curves for stainless steel alloys. *J. Constr. Steel Res.* 59 (1), 47–61.
- Rossi, B., Jaspert, J.P., Rasmussen, K.J., 2010. Combined distortional and overall flexural-torsional buckling of cold-formed stainless steel sections: experimental investigations. *J. Struct. Eng.* 136 (4), 354–360.
- Saliba, N., Gardner, L., 2013. Cross-section stability of lean duplex stainless steel welded I-sections. *J. Constr. Steel Res.* 80, 1–14.
- SEI/ASCE 8-02, 2002. Specification for the Design of Cold-Formed Stainless Steel Structural Members. American Society of Civil Engineers (ASCE), Reston.
- Shamass, R., Cashell, K.A., 2019. Analysis of stainless steel-concrete composite beams. *J. Constr. Steel Res.* 152, 132–142.
- Sharifi, Y., Tohidi, S., Paik, J.K., 2016. Ultimate compressive strength of deteriorated steel web plate with pitting and uniform corrosion wastage. *Sci. Iran.* 23 (2), 486–499.
- Sharifi, Y., Moghbeli, A., Hosseinpour, M., Sharifi, H., 2019. Study of neural network models for the ultimate capacities of cellular steel beams. *Iranian Journal and Science and Technology, Transactions of Civil Engineering* 44, 579–589.
- Sharifmousavi, S.S., Borhani, M.S., 2020. Support vectors machine-based model for diagnosis of multiple sclerosis using the plasma levels of selenium, vitamin B12, and vitamin D3. *Inform. Med. Unlocked* 20, 100382.
- Shu, G., Zheng, B., Shen, X., 2013. Experimental and theoretical study on the behavior of cold-formed stainless steel stub columns. *International Journal of Steel Structures* 13, 141–153.
- Smola, A.J., Schölkopf, B., 2004. A tutorial on support vector regression. *Stat. Comput.* 14, 199–222.
- Syarif, I., Prugel-Bennett, A., Wills, G., 2016. SVM parameter optimization using grid search and genetic algorithm to improve classification performance. *TELKOMNIKA (Telecommunication Computing Electronics and Control)* 14 (4), 1502–1509. <https://doi.org/10.12928/telkomnika.v14i4.3956>.
- Theofanous, M., Gardner, L., 2010. Experimental and numerical studies of lean duplex stainless steel beams. *J. Constr. Steel Res.* 66 (6), 816–825.
- Theofanous, M., Liew, A., Gardner, L., 2015. Experimental study of stainless steel angles and channels in bending. In: *Structures*, 4. Elsevier, pp. 80–90.
- Toffolon, A., Kraus, M.A., Taras, A., 2021. Deep Learning based method for the prediction of the buckling resistance of SHS and RHS. *ce/papers* 4 (2–4), 1076–1084.
- Tohidi, S., Sharifi, Y., 2014. Inelastic lateral-torsional buckling capacity of corroded web opening steel beams using artificial neural networks. *IES J. Part A Civ. Struct. Eng.* 8, 24–40.
- Tohidi, S., Sharifi, Y., 2015. Inelastic lateral-torsional buckling capacity of corroded web opening steel beams using artificial neural networks. *IES J. Part A Civ. Struct. Eng.* 8 (1), 24–40.
- Tohidi, S., Sharifi, Y., 2016. Load-carrying capacity of locally corroded steel plate girder ends using artificial neural network. *Thin-Walled Struct.* 100, 48–61.
- Vapnik, V., 1995. *The Nature of Statistical Learning Theory*. Springer science & business media.
- Vapnik, V., 1998. *Statistical Learning Theory*, second ed., Vol. 1. Wiley, New York, p. 624.
- Vapnik, V.N., 1999. An overview of statistical learning theory. *IEEE Trans. Neural Network.* 10 (5), 988–999.
- Wei, J., He, X., 2023. Support vector regression model with variant tolerance. *Measurement and Control*, 00202940231180620. <https://doi.org/10.1177/00202940231180620>.
- Xu, Y., Zhang, M., Zheng, B., 2021. Design of cold-formed stainless steel circular hollow section columns using machine learning methods. In: *Structures*, 33. Elsevier, pp. 2755–2770.
- Xu, Z., Lv, Z., Chu, B., Sheng, Z., Li, J., 2024. Progress and prospects of future urban health status prediction. *Eng. Appl. Artif. Intell.* 129, 107573.
- Yang, Y., Niu, S., Zhi, X., 2023. DSM formula for local-global interaction buckling of cold-formed stainless steel I-beams. *Sustainability* 15 (2), 1333.
- Young, B., Hartono, W., 2002. Compression tests of stainless steel tubular members. *J. Struct. Eng.* 128 (6), 754–761.
- Yuan, H.X., Wang, Y.Q., Shi, Y.J., Gardner, L., 2014. Stub column tests on stainless steel built-up sections. *Thin-Walled Struct.* 83, 103–114.
- Zarringol, M., Thai, H.T., Naser, M.Z., 2021. Application of machine learning models for designing CFCFST columns. *J. Constr. Steel Res.* 185, 106856.
- Zhao, O., Gardner, L., Young, B., 2016a. Structural performance of stainless steel circular hollow sections under combined axial load and bending – Part 1: experiments and numerical modelling. *Thin-Walled Struct.* 101, 231–239. <https://doi.org/10.1016/j.tws.2015.12.003>.
- Zhao, O., Gardner, L., Young, B., 2016b. Structural performance of stainless steel circular hollow sections under combined axial load and bending—Part 2: parametric studies and design. *Thin-Walled Struct.* 101, 240–248. <https://doi.org/10.1016/j.tws.2015.12.005>.
- Zhao, O., Gardner, L., Young, B., 2016c. Testing and numerical modelling of austenitic stainless steel CHS beam-columns. *Eng. Struct.* 111, 263–274. <https://doi.org/10.1016/j.engstruct.2015.12.035>.
- Zhou, F., Young, B., 2005. Tests of cold-formed stainless steel tubular flexural members. *Thin-Walled Struct.* 43 (9), 1325–1337.